

**ON DAMAGE EVOLUTION OF
PEM ELECTRODES**

by

Melissa C. Lugo

A thesis submitted to the Faculty of the University of Delaware in partial fulfillment of the requirements for the degree of Master of Science in Mechanical Engineering

Summer 2010

Copyright 2010 Melissa C. Lugo
All Rights Reserved

**ON DAMAGE EVOLUTION OF
PEM ELECTRODES**

by

Melissa C. Lugo

Approved: _____
Anette M. Karlsson, Ph.D.
Professor in charge of thesis on behalf of the Advisory Committee.

Approved: _____
Anette M. Karlsson, Ph.D.
Chair of the Department of Mechanical Engineering

Approved: _____
Michael J. Chajes, Ph.D.
Dean of the College of Engineering

Approved: _____
Debra Hess Norris, M.S.
Vice Provost for Graduate and Professional Education

ACKNOWLEDGMENTS

I would like to express my sincere gratitude to my advisors, Dr. Anette M. Karlsson and Dr. Michael H. Santare, for their guidance, support, and excellent contribution to this work.

Special thanks to Dr. Joshua Hertz for his willingness to help me through this process and for being part of my defense committee.

I would also like to thank all my lab-mates for their professional support and friendship: Dr. Yaliang Tang, Dan Cojocar, Ahmet Kusoglu, Mercedes Hernandez, Vasan Chandrasekaran, Liang Chen, Narinder Khattr, Yun Wang, Zongwen Lu, and Tom Cender.

Last, but not least, I would like to thank my family for being the center of my life and the constant motivation to pursue new challenges.

TABLE OF CONTENTS

| | |
|---|-----------|
| LIST OF TABLES..... | 6 |
| LIST OF FIGURES | 7 |
| ABSTRACT | 11 |
| Chapter | |
| 1. INTRODUCTION | 13 |
| 1.1 Polymer Electrolyte Membrane Fuel Cells..... | 13 |
| 1.2 Tensile Test of membrane A | 18 |
| 1.3 Thesis Outline..... | 23 |
| 2. EXPERIMENTAL WORK | 26 |
| 2.1 Test-to-failure of MEAs | 26 |
| 2.2 Interrupted Test..... | 30 |
| 2.2.1 Problem Description..... | 30 |
| 2.2.2 Material Studied and Experimental Set-Up..... | 31 |
| 2.2.3 Scanning Electron Microscope (SEM)..... | 32 |
| 2.2.4 Results and Discussion..... | 33 |
| 2.3 Synopsis..... | 37 |
| 3. NUMERICAL WORK..... | 38 |
| 3.1 Model Description..... | 38 |
| 3.1.1 Introduction | 38 |
| 3.1.2 Geometry | 39 |
| 3.1.3 Constitutive Equations | 44 |
| 3.1.4 Cases Studied | 45 |
| 3.1.4.1 Influence of Plasticity..... | 46 |
| 3.1.4.2 Influence of Crack Density..... | 48 |
| 3.1.4.3 Influence of Crack Length | 51 |

| | | |
|-----------|---|-----------|
| 3.1.4.4 | Influence of Interfacial Delamination..... | 52 |
| 3.2 | Results and Discussion..... | 54 |
| 3.2.1 | Influence of Plasticity in the Electrode..... | 55 |
| 3.2.2 | Influence of Crack Density..... | 57 |
| 3.2.3 | Influence of Crack Length..... | 60 |
| 3.2.4 | Influence of Interfacial Delamination..... | 62 |
| 3.2.5 | Combined Effects..... | 63 |
| 3.3 | Synopsis..... | 67 |
| 4. | CONCLUSIONS..... | 69 |
| | REFERENCES..... | 73 |

LIST OF TABLES

| | | |
|-----------|---|----|
| Table 2.1 | Observations from SEM images at selected strain levels..... | 36 |
| Table 3.1 | Isotropic hardening values for membrane A based on tensile test results..... | 45 |
| Table 3.2 | Values for Young's Modulus and Yield Stress. | 46 |
| Table 3.3 | Plasticity with strain hardening properties for the membrane and the electrode, where σ_y and ϵ_p indicate the yield strength and plastic strain respectively. These values are used as input in the finite element code..... | 47 |
| Table 3.4 | Different values considered for crack length..... | 52 |
| Table 3.5 | Different values considered for the interfacial delamination length..... | 54 |

LIST OF FIGURES

| | | |
|------------|---|----|
| Figure 1.1 | Technological issues in PEMFCs..... | 14 |
| Figure 1.2 | Schematic of PEMFC and its components. | 15 |
| Figure 1.3 | Tensile test setup. The grips keep the specimen aligned with the extension rod. | 19 |
| Figure 1.4 | Experimental results for membrane A at T=25°C and RH=30%, showing stress as a function of strain for 5 tested specimens (machine direction) (machine direction). Experimental data is taken from ref. [9]. | 21 |
| Figure 1.5 | Experimental results for membrane A at T=25, 45, 65, and 85°C at 50% RH, showing stress as a function of strain (machine direction). Experimental data is taken from ref. [9]. | 22 |
| Figure 1.6 | Experimental results for membrane A at 30, 50, 70, and 90% RH at T=45°C, showing stress as a function of strain (machine direction). Experimental data is taken from ref. [9]. | 24 |
| Figure 2.1 | Experimental results for the MEA at T=25°C and RH=30%, showing stress as a function of strain for 5 tested specimens (machine direction) | 28 |
| Figure 2.2 | Tensile test results for the MEA at various temperature and relative humidity combinations, showing force as a function of displacement (machine direction). | 29 |
| Figure 2.3 | Sample of MEA (black) used to conduct an interrupted test. Rectangular piece of dimensions: 110 mm in length and 10 mm in width..... | 31 |
| Figure 2.4 | Aluminum stubs used for taking SEM images. | 33 |
| Figure 2.5 | SEM image of an untested (as received) MEA sample..... | 34 |

| | | |
|------------|--|----|
| Figure 2.6 | SEM image of an MEA sample pulled until 0.2 strain. The cracks are perpendicular to loading direction..... | 35 |
| Figure 2.7 | SEM images of MEA samples pulled until different strain levels: a) 0.2 strain, b) 0.3 strain, and c) 0.4 strain. Crack density increases as the tension load is applied. | 35 |
| Figure 2.8 | SEM image of an MEA sample pulled until 0.4 strain. Separation between cracks and width of the cracks are illustrated. | 36 |
| Figure 3.1 | Schematic representation of a single fuel cell and the model investigated. A quarter of the geometry of the MEA is used in the numerical analysis. Mechanical boundary conditions are shown. A constant displacement is applied on the right edge of the cell. | 40 |
| Figure 3.2 | Schematic representation of the finite element model and its corresponding dimensions..... | 41 |
| Figure 3.5 | Tensile test results for MEA and Membrane at T=25°C and RH=30%..... | 48 |
| Figure 3.6 | Plasticity with strain hardening response assumed for the electrode following the response of the MEA and the membrane respectively..... | 49 |
| Figure 3.7 | Finite element models of MEA generated for studying the influence of crack density on the mechanical response: a) 4 Cracks per mm, b) 32 Cracks per mm, c) 64 Cracks per mm, d) 128 Cracks per mm..... | 51 |
| Figure 3.8 | Finite element models of MEA generated for studying the influence of crack length on the mechanical response: a) $L_{crack} = 13.75\% W_{MEA}$, b) $L_{crack} = 27.50\% W_{MEA}$, c) $L_{crack} = 55\% W_{MEA}$, d) $L_{crack} = 58\% W_{MEA}$, e) $L_{crack} = 61\% W_{MEA}$, f) $L_{crack} = 63.50\% W_{MEA}$, g) $L_{crack} = 72\% W_{MEA}$, h) $L_{crack} = 80\% W_{MEA}$. (L_{crack} = Crack Length, W_{MEA} = Width of MEA) | 53 |
| Figure 3.9 | Finite element models of MEA generated for studying the influence of interfacial delamination length on the mechanical response: a) $L_{delam.} = 2.70\% L_{MEA}$, b) $L_{delam.} = 5.40\% L_{MEA}$, c) $L_{delam.} = 20\% L_{MEA}$, d) $L_{delam.} = 40\% L_{MEA}$ | 55 |

| | | |
|-------------|---|----|
| Figure 3.10 | Comparison between experimental and numerical results. Numerical curves show the influence of introducing plasticity in the electrodes on the mechanical response of MEA. Numerical model with no cracks..... | 56 |
| Figure 3.11 | Force as a function of displacement from the numerical simulations showing the influence of crack density in the mechanical response of the MEA. Hardening properties for electrodes are assumed based on the constitutive response of the membrane. | 57 |
| Figure 3.12 | Comparison between experimental and numerical results showing force as a function of displacement. Numerical curves show the influence of crack density in the mechanical response of the MEA. Hardening properties for electrodes are assumed to follow the constitutive response of the membrane | 59 |
| Figure 3.13 | Comparison between experimental and numerical results showing force as a function of displacement. Numerical curves show the influence of crack density in the mechanical response of MEA. Electrodes are assumed perfectly plastic..... | 60 |
| Figure 3.14 | Comparison between experimental and numerical results showing force as a function of displacement. Numerical results show the influence of crack length on the mechanical response of the MEA. The numerical curves with solid lines show the influence of cracks through the electrode. The numerical curves with dash lines show the influence of cracks through electrode and membrane. A numerical model with 32 cracks and hardening properties, based on the constitutive behavior of the membrane, for electrodes are assumed..... | 61 |
| Figure 3.15 | Comparison between experimental and numerical results showing force as a function of displacement for various delamination lengths. Numerical model with 32 cracks and hardening properties, based on the constitutive response of the membrane, for electrodes are assumed..... | 63 |
| Figure 3.16 | Comparison between experimental and numerical results showing force as a function of displacement. Numerical results show the influence of crack density and mechanical properties of the electrodes on the MEA mechanical response..... | 64 |

Figure 3.17 Comparison between experimental and numerical results showing force as a function of displacement. Numerical curves show the influence of crack density, interfacial delamination length, and plasticity properties on the mechanical response of MEA, where $L_{del} = 40\% L_{MEA}$ 66

ABSTRACT

One of the main challenges that the polymer electrolyte membrane (PEM) fuel cell industry faces is the improvement of the durability of its fuel cells. PEMFCs are required to last for long periods of time and in order to achieve this demand, it is necessary to better understand and improve the durability of the membrane electrode assembly (MEA), which is a critical component of a PEM fuel cell. To address this issue, the failure evolution and the mechanical properties of PEM electrodes are investigated through experimental and numerical work. From an experimental point of view, the failure evolution of PEM electrodes is examined by conducting strain controlled interrupted tests. The evolution of distinct defects, such as cracks, on the surface of the electrodes is then analyzed by using scanning electron microscope. It is very important to consider the evolution of cracks observed on the electrodes, in order to capture the mechanical response of the MEA. The mechanical behavior of the MEA is obtained by conducting tensile tests at various temperature and humidity conditions. After obtaining experimental data, finite element simulations are performed by using the software ABAQUS, where the mechanical properties of “membrane A” and the electrodes are used as input. Reverse analysis is used in order to establish the mechanical properties of the electrodes that lead to the experimentally measured response of the MEA. Different cases are investigated numerically including the influence of plasticity in the electrodes, crack density, crack length, and interfacial delamination. The numerical results are compared with the experimental results from the MEA. The results indicate that crack density has a profound effect on the mechanical behavior of the MEA and it dominates over other factors such as the

mechanical properties of the electrodes and the length of delamination. The combination of experimental and numerical work resulted in a powerful approach to determine the mechanical properties of PEM electrodes. In addition, it contributed to better understand the different factors that affect the mechanical degradation of MEAs and PEM electrodes, and consequently the durability of PEMFCs.

Chapter 1

INTRODUCTION

1.1 Polymer Electrolyte Membrane Fuel Cells

Fuel cells are electrochemical devices that convert chemical energy directly into electrical work [1]. In general, there are several types of fuel cells currently under development, each with its own advantages, limitations, and potential applications. This work is focused on Polymer Electrolyte Membrane Fuel Cells (PEMFCs), also known as Proton Exchange Membrane Fuel Cells (PEMFCs). This kind of fuel cell is an alternative power source being developed for stationary, portable, and transportation applications. PEMFCs, compared to other types of fuel cells, can deliver higher power density and have lower weight and volume. However, there are several issues that currently prevent the widespread commercialization of PEMFCs. For transportation applications, durability, high efficiency, rapid start-up, and compact size are some of the primary technical issues [1].

Potential advantages make PEMFC an excellent candidate for different applications. Currently, a number of research studies are being developed to aid in the push toward commercialization. One of the primary advantages of PEMFCs is the low temperature operation that allows them to start quickly and operate in subfreezing temperature, although normal operating temperatures are 20-90°C [1]. Moreover, for transportation applications, their high energy density and high efficiency with low pollution is an important benefit of PEMFCs. Less dependence on oil and its effects on

the world economy is also a strong driver toward development of fuel cell vehicles [1, 2, 3].

However, before widespread commercialization of PEMFC can be realized, some technological issues, that complicate performance and control, have to be addressed. Figure 1.1 shows some of the technological hurdles that need to be solved in order to improve the marketability of PEMFCs. Some of these issues are cost, startup time, reliability and durability, power density, hydrogen storage and distribution, water and heat management.

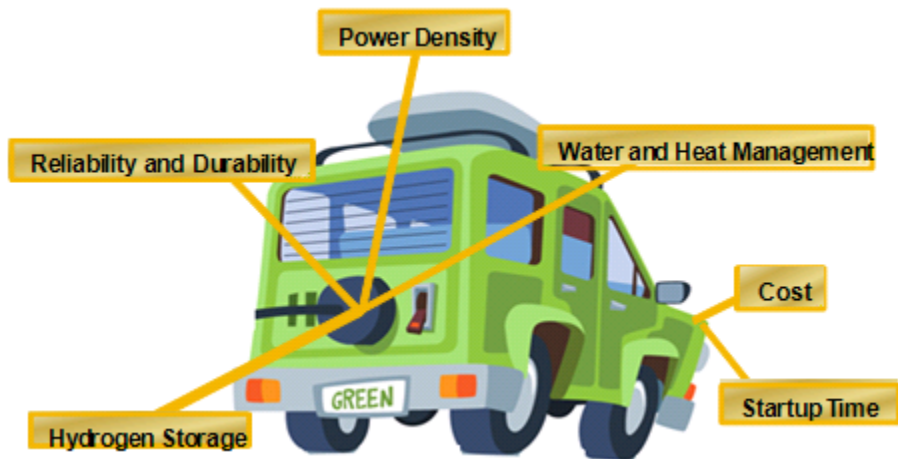


Figure 1.1 Technological issues in PEMFCs

The heart of the fuel cell system is the fuel cell stack. A fuel cell stack is a set of individual cells connected in series and/or parallel (Fig. 1.2). Other components necessary for fuel cell system operation include subsystems for fuel delivery, voltage regulation, stack temperature control, separate humidification systems, etc. [1]. In

order to operate, this type of fuel cell needs only hydrogen, oxygen from the air, and water. Typically, pure hydrogen is supplied from storage tanks or onboard reformers. PEM fuel cells operate at relatively low temperatures, around 80°C (176°F) [2].

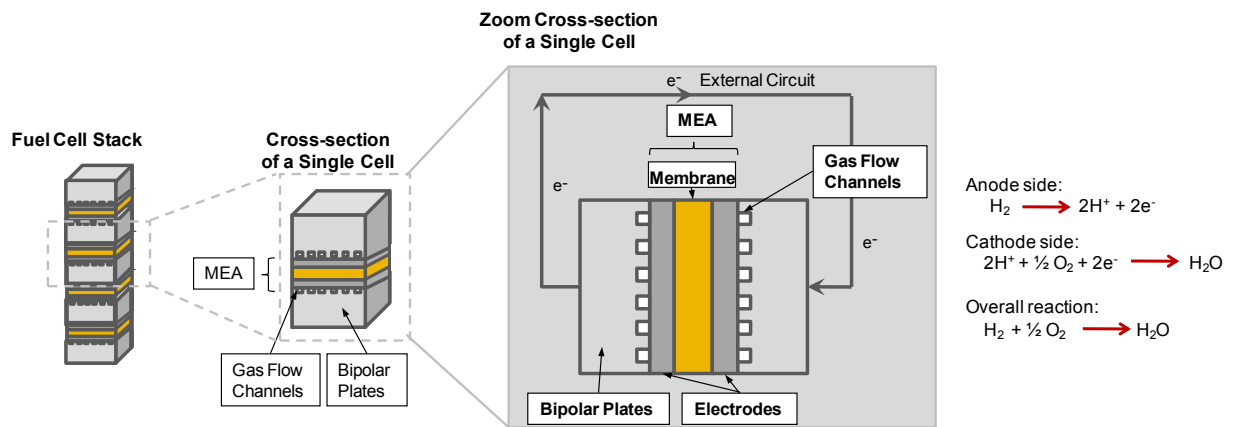
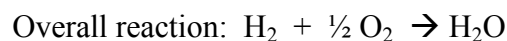
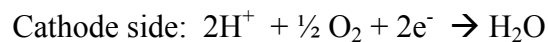


Figure 1.2 Schematic of PEMFC and its components.

In general, a single cell in a PEMFC is made from several layers of different materials. This work entails studies of the membrane electrode assembly (MEA), which is a key component of PEMFCs (Fig. 1.2). The MEA is a layered structure containing a membrane made of a polymer (electrolyte) and two electrodes (anode and cathode) that are porous carbon electrodes containing a platinum catalyst. Each of the electrodes is coated onto one side with a catalyst layer that facilitates the chemical reaction at that electrode [1, 2]. These three components (membrane, anode, cathode) are typically formed together into a single component, known as the membrane electrolyte assembly (MEA). The polymer electrolyte membrane (PEM)

conducts the positively charged hydrogen ions (protons) and blocks the electrons. The PEM is a key component of the fuel cell. It must permit only the hydrogen ions to pass between the anode and cathode. Other substances passing through the electrolyte would disrupt the chemical reaction and adversely affect the operation of the fuel cell. The negatively charged side of the fuel cell is the anode which conducts away the electrons that are freed from the hydrogen molecules. These electrons flow through an external circuit. The cathode is the positive side of the fuel cell which conducts the electrons back from the external circuit to the catalyst [2].

The chemical processes occurring during the operation of a PEMFC are basically as follow: hydrogen gas passes over the anode, and with the help of a catalyst, separates into electrons and protons (hydrogen ions). The protons flow to the other electrode (cathode) through the membrane while the electrons flow through an external circuit, thus creating electric current. The protons and electrons combine with the oxygen, which is flowing through the cathode, and produce water [4]. The overall reaction that takes place in the fuel cell is the sum of the anode and cathode reactions, that is, the combination of hydrogen with oxygen to produce water (Fig.1.2). The chemical formulas are:



This research addresses the durability issue. Significant improvements in durability of PEMFCs must be achieved in order to make them competitive with automotive combustion engines and stationary power generation systems. Toward this goal, the automotive fuel cell must achieve 5,500 h of operating lifetime, while a

stationary fuel cell must operate nearly continuously for over 40,000 h. These requirements are significant challenges considering that the cell can suffer degradation due to load cycling, changes in external temperature conditions, etc. [1]. Currently, the use of PEMFC is limited due to premature failures. Better understanding of the failure mechanisms in PEMFCs is crucial in order to predict and improve their performance and lifetime. Several phenomena are involved in the degradation of PEMFC. In a fuel cell, the membrane electrode assembly is a component which presents a variety of degradation modes ranging from chemical, mechanical, and thermal degradation [7, 12]. The different issues affecting MEA degradation are: manufacturing, design, assembly, material properties, and operating conditions [7]. These factors determine the degradation and failure mechanism.

Major defects such as cracks, delamination, thickness variations, etc. have been identified in unused and used samples of MEA. [7, 8]. Enlargement of these initial cracks can be induced by mechanical stresses, as a result of fuel cell operation and changes in the MEA environment [13]. One of the major causes of PEMFC's degradation is the mechanical stress in the membrane [5, 6, 10]. In previous work [10], it was seen that the temperature gradient in the MEA causes nonuniform distribution of stresses, which can lead to delamination between the membrane and the electrodes. Consecutive swellings and contractions of the membrane due to hygro-thermal cycles induce cyclical mechanical stresses that may cause cracking [7]. Results from fuel cell durability experiments [8], indicate that cracks typically appear in areas where the MEA is mechanically and thermally most stressed. The characterization of the mechanical properties of the membrane as function of temperature and relative humidity has been investigated in recent studies [9]. The use of these properties as

input in finite element models has enabled the prediction of stresses within the membrane during hygro-thermal cycles [10, 11]. These mechanical stresses can lead to plastic deformations of the MEA, which in turn, can lead to the formation of cracks, and to delamination between the membrane and the electrodes [7, 8]. In summary, according to numerous studies, MEA's durability is limited by mechanical failures, which arise due to operating conditions such as temperature, humidity, freeze-thaw cycling, etc. and these failures are influenced by the mechanical properties of the MEA components [14].

1.2 Tensile Test of membrane A

The material properties and mechanical response of polymer electrolyte membrane was investigated in ref. [9] by conducting tensile tests under real life operating conditions. The experimental procedure and results from these tests will be summarized in this section. A tensile test is probably the most fundamental type of mechanical test that can be performed on a material. By pulling on a specimen, it is possible to determine how the material will react to forces being applied in tension. In previous work [9], several membranes were tested this way including the membrane, referred to as "Membrane A", which is an experimental membrane developed by W.L. Gore & Associates. The Membrane A is a perfluorosulfonic acid membrane (PFSA) with e-PTFE reinforcement. The properties obtained in these tensile tests are used in chapter 3 and reviewed here for completeness.

The tensile tests were conducted using an MTS Alliance TM RT/5 tensile tester (Fig. 1.3) fitted with an ESPEC environmental control chamber. Membrane A has two distinct in-plane directions due to the manufacturing process: machine and transverse direction. The experiments were conducted in both directions to investigate

possible differences in properties. Selected mechanical properties (Young's modulus and proportional limit stress) were evaluated at selected temperature and relative humidity conditions. Previous studies [10, 11, 15] showed that the mechanical properties of the membrane are strongly dependent on the environmental conditions (temperature and relative humidity).

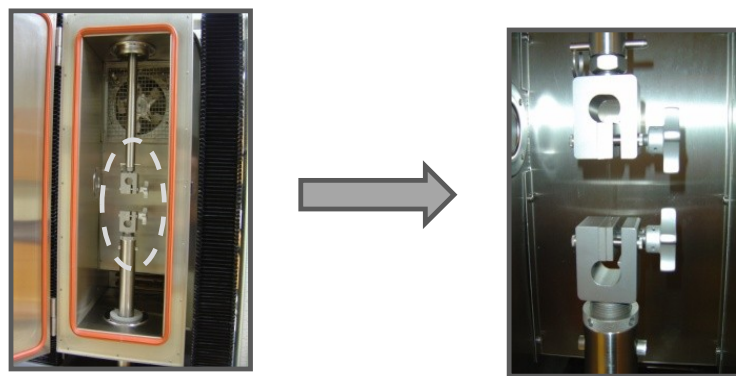


Figure 1.3 Tensile test setup. The grips keep the specimen aligned with the extension rod.

The tests were conducted at selected temperature and humidity combinations, with temperatures ranging from 25 to 85°C and with relative humidities ranging from 30 to 90%. Several specimens were tested at each temperature and humidity combination. The specimens were cut from “Membrane A” sheets, which were produced by W.L. Gore & Associates with a nominal thickness of 20 μm . The samples were cut into rectangular pieces of 110 mm in length and 10 mm in width. They were carefully measured using a caliper to obtain the length and the width, and using a micrometer to measure the thickness. After the sample was measured, it was

mounted in the tensile tester by clamping it in a pair of vise-action grips. The environmental control chamber was used to set the desired temperature and relative humidity. During the displacement-controlled tensile testing, the force as a function of displacement was recorded. From this force-displacement data, the stress-strain curve for the test was calculated. This curve was used to determine Young's modulus and proportional limit stress for each temperature and humidity combination. Figure 1.4 shows the experimental stress-strain results for Membrane A at $T=25^{\circ}\text{C}$ and $\text{RH}=30\%$. The curves represent each of the specimens tested at this condition and show the typical scatter from the experiments.

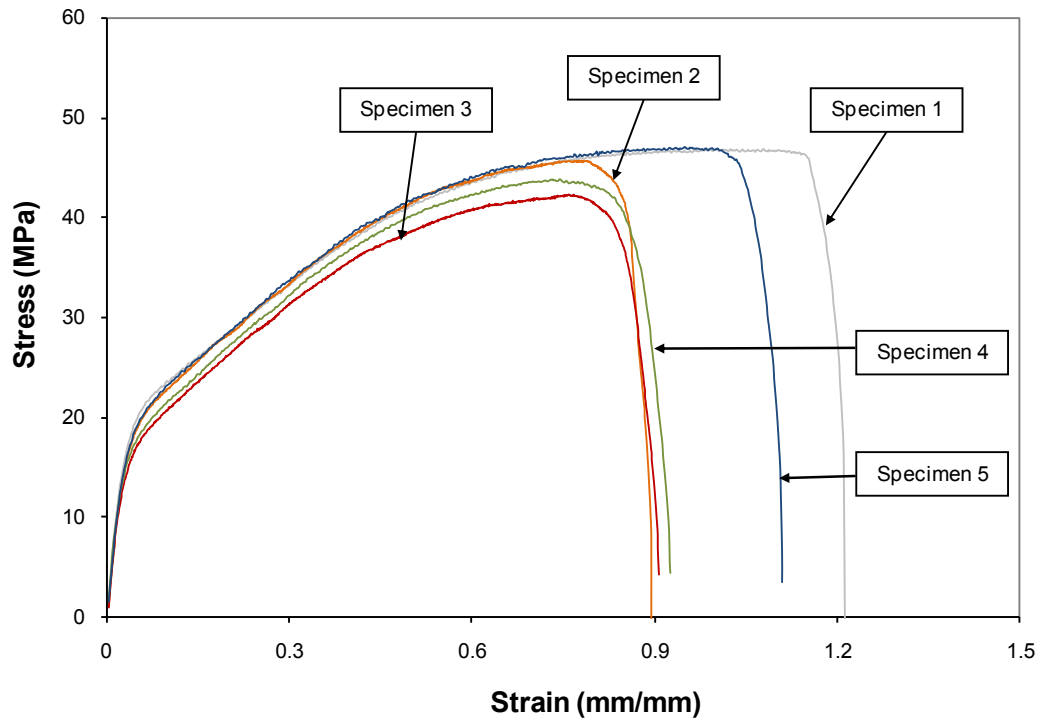


Figure 1.4 Experimental results for membrane A at $T=25^{\circ}\text{C}$ and $\text{RH}=30\%$, showing stress as a function of strain for 5 tested specimens (machine direction) (machine direction). Experimental data is taken from ref. [9].

Figure 1.5 shows the experimental results for Membrane A at 50% RH and selected temperatures (25, 45, 65, and 85°C), displaying stress as a function of strain. The results from this work show that Young's modulus and proportional limit stress are significantly affected by temperature and both decrease with increasing temperature.

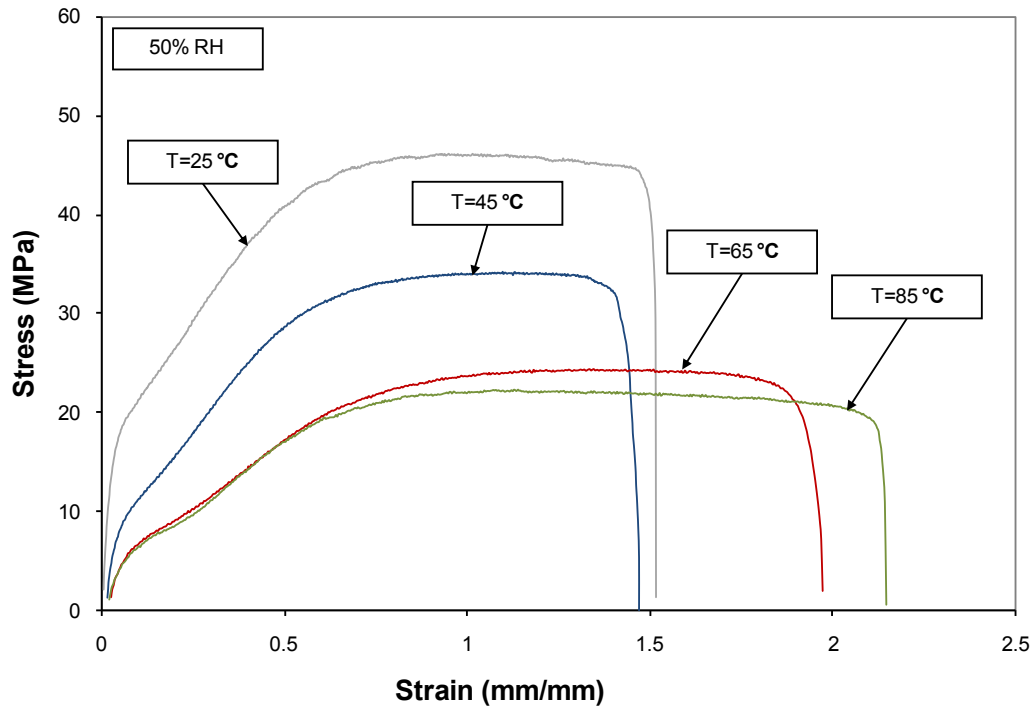


Figure 1.5 Experimental results for membrane A at $T=25, 45, 65,$ and 85°C at 50% RH, showing stress as a function of strain (machine direction). Experimental data is taken from ref. [9].

In addition, figure 1.6 shows the experimental stress-strain results for Membrane A at 45°C and selected relative humidities (30, 50, 70, and 90%). The graph shows that Young's modulus and proportional limit stress decrease with increasing relative humidity. Figs. 1.4 and 1.5 suggest that when Membrane A is subjected to a high temperature and humidity, the mechanical properties are significantly affected. By performing these experimental tests, the mechanical properties of Membrane A were established and the effect that environmental

conditions (temperature and relative humidity) have on the mechanical response was investigated. Based on this experimental work [9], numerical simulations, using the finite element method, were conducted in order to establish the mechanical properties of PEM electrodes. The numerical work will be discussed in chapter 3.

1.3 Thesis Outline

Durability of polymer electrolyte membrane fuel cells (PEMFCs) is one of the current limitations preventing the widespread commercialization of this technology. Determination, understanding, and quantification of the degradation mechanisms are necessary steps for increasing PEMFC's lifetime and potential commercial competitiveness. Though there are many parts of a PEMFC that can influence the durability, this work focuses on the mechanical degradation of the membrane electrode assembly, and in particular of PEM electrodes.

This work has its roots in previous experimental work [9], where the mechanical properties of the "Membrane A" were determined. "Membrane A" is an experimental membrane developed by W.L. Gore & Associates. An extension of the previous work is presented here, where MEAs based on Membrane A are investigated. In order to understand and model the deformation and fracture behavior, it is necessary to quantify the evolution of microstructural damage processes, such as cracks and delaminations. This problem is addressed in Chapter 2, where an interrupted testing technique is presented in addition to tests-to-failure of the MEAs. A strain controlled interrupted test is conducted for the MEAs to explore the influence of load and the morphological parameters on damage. This test is performed at different strain levels under uniaxial tension in order to incorporate different damage levels. Moreover, tensile tests are conducted on MEAs in order to establish the mechanical properties

(Young's modulus and proportional limit stress). Results from interrupted tests and tests-to-failure of MEAs are shown.

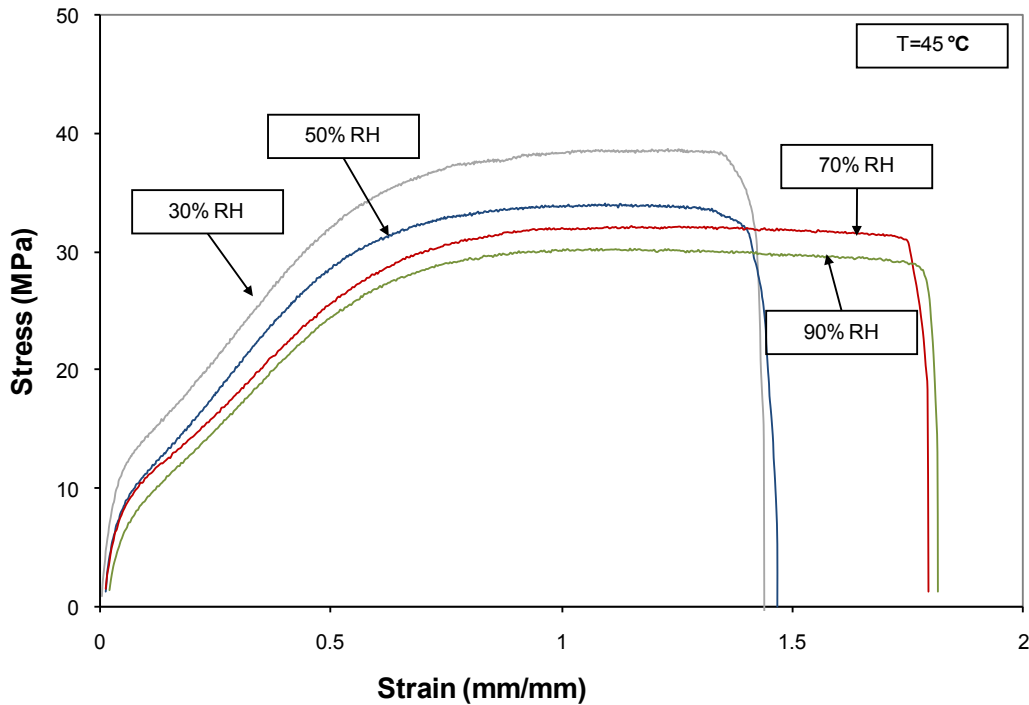


Figure 1.6 Experimental results for membrane A at 30, 50, 70, and 90% RH at $T=45^{\circ}\text{C}$, showing stress as a function of strain (machine direction). Experimental data is taken from ref. [9].

From tensile test results [9], the mechanical response of Membrane A, under various environmental conditions, has been established, exhibiting a high non-linear behavior. In addition, in Chapter 2 the failure evolution and mechanical properties of MEAs based on Membrane A are investigated. Based on these results, in

Chapter 3 a finite element model is developed to study different mechanical effects: influence of plasticity in the electrodes, influence of crack density, influence of crack length, and influence of interfacial delamination. The overall objective is to investigate the failure evolution and mechanical properties of PEM electrodes by using finite element analysis in conjunction with experimental results. These numerical simulations show good agreement with experimental data in the linear elastic region and the beginning of the plastic deformation. Results for selected cases are shown.

To improve the durability and lifetime of PEMFCs requires better understanding of the failure mechanisms and establishing of the mechanical properties of the MEA and its components. By combining experimental and numerical work, it is possible to address these issues. The constitutive behavior of the MEA with damage can be described by fitting experimental and numerical results. This work attempts to predict failure in order to improve the long-term performance of PEMFCs.

Chapter 2

EXPERIMENTAL WORK

2.1 Test-to-failure of MEAs

Fuel cell operation and changes in the MEA environment can lead to premature failures that reduce performance and lifetime. The study of the mechanical properties of the MEA and its components is crucial to improve the durability of PEMFC. In previous work [9], discussed in chapter 1, the mechanical properties of Membrane A were established by conducting tensile tests at various temperature and relative humidity combinations. The results from these experiments show that the mechanical response of Membrane A is dependent on operating conditions. Since our work is focused on the MEA and its components (membrane and electrodes), additional experimental tests are required in order to investigate the mechanical properties of the MEA. Establishing the mechanical properties of the MEA and Membrane A are necessary steps to determine the mechanical properties of PEM electrodes, since the electrodes do not exist in a form that can be tested by themselves.

The tensile testing technique is the experimental approach used to investigate the mechanical properties and response of the MEA under environmental conditions simulating real life operating conditions. The MEA (membrane electrode assembly) was developed by W.L. Gore & Associates from a polymer electrolyte membrane, referred as Membrane A, which properties have been investigated in previous work [9]. Two distinct in-plane directions results due to the manufacturing

process: the machine and transverse directions. The MEA experiments were conducted in both directions to investigate possible differences in properties. The tensile tests were conducted in collaboration with Dr. Yaliang Tang using an MTS Alliance TM RT/5 tensile tester (Fig. 1.3) fitted with an ESPEC environmental control chamber. The tests were conducted at various temperature and humidity combinations, with temperatures ranging from 25 to 85°C and with relative humidities ranging from 30 to 90%. Several specimens were tested at each temperature and humidity combination. The procedure used to measure, cut, and set the specimens in the tensile tester is the same as the one used for the Membrane A tensile tests (explained in chapter 1). Selected mechanical properties (Young's modulus and proportional limit stress) were evaluated at selected temperature and relative humidity conditions. During the tensile testing, the force as a function of displacement was recorded and the stress-strain curve was calculated from this data. This relationship was used to determine Young's modulus and proportional limit stress for each temperature and humidity combination. Figure 2.1 shows the experimental results for the MEA at T=25°C and RH=30%, displaying stress as a function of strain. The curves represent each of the specimens tested at this condition and show the typical scatter in the experimental measurements.

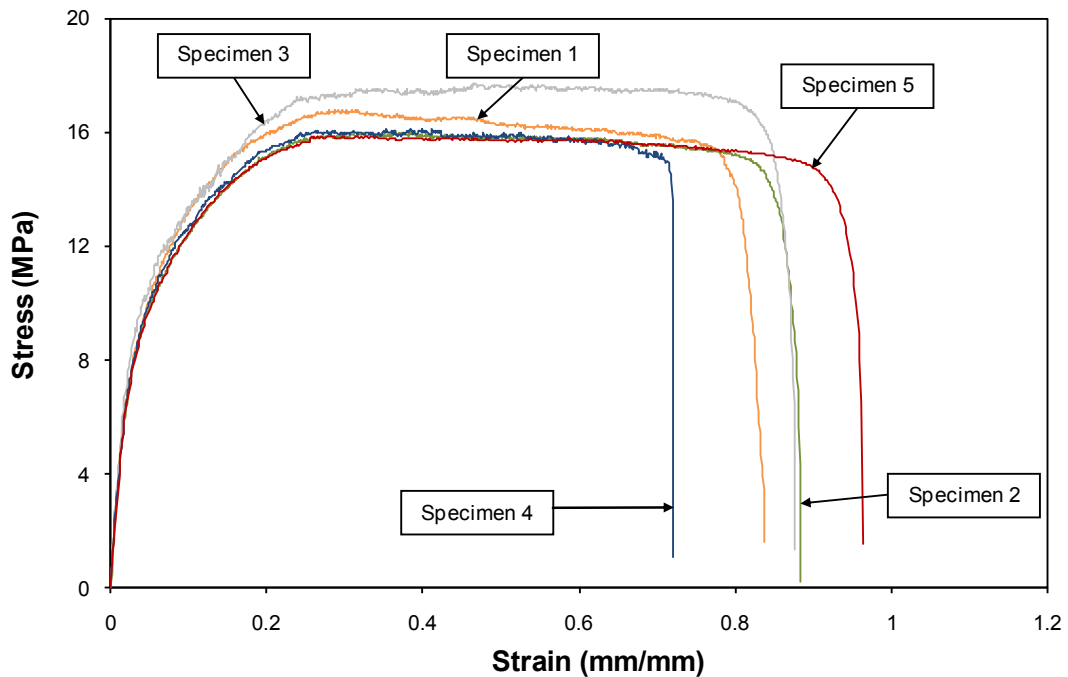


Figure 2.1 Experimental results for the MEA at $T=25^{\circ}\text{C}$ and $\text{RH}=30\%$, showing stress as a function of strain for 5 tested specimens (machine direction).

Figure 2.2 shows the experimental results for the MEA at various temperature and relative humidity combinations, displaying force as a function of displacement. The results from this work show that Young's modulus and proportional limit stress both decrease as temperature or relative humidity increase. These results suggest that when the MEA is subjected to a high temperature and humidity simultaneously, the mechanical properties are significantly affected. By conducting separate tensile tests, the mechanical properties of the Membrane A [9] and the MEA have been individually determined. Based on the mechanical properties obtained from

the MEA and Membrane A tensile tests, numerical simulations can be conducted to indirectly determine the mechanical properties of PEM electrodes. The numerical work, utilizing the finite element method, will be discussed in chapter 3.

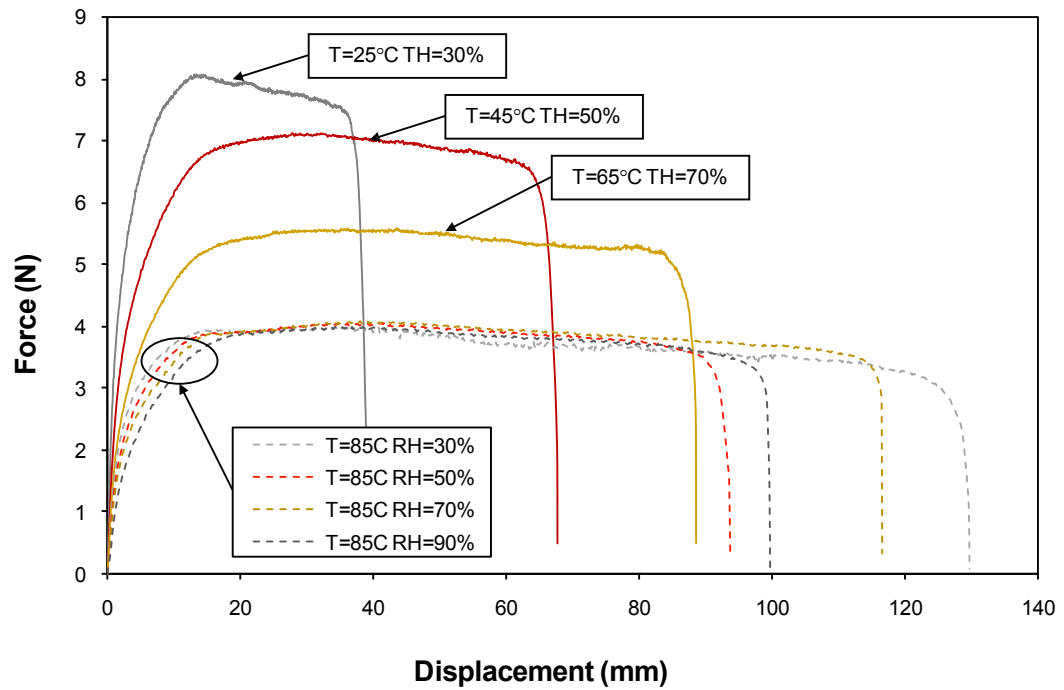


Figure 2.2 Tensile test results for the MEA at various temperature and relative humidity combinations, showing force as a function of displacement (machine direction).

2.2 Interrupted Test

2.2.1 Problem Description

Efforts at improving the lifetime of PEM fuel cells will require better understanding of the failure mechanisms. Failure in fuel cell systems may occur in several ways such as chemical degradation, mechanical damage, etc. This project entails the study of the mechanical damage in polymer electrolyte membrane fuel cells (PEMFCs). In particular, this work is focused on the Membrane Electrode Assembly (MEA). In order to investigate the failure evolution in MEA, interrupted tension tests were conducted and SEM images were taken to obtain information about the damage development.

Interrupted testing is an experimental approach used to study the evolution of microscopic damage that can lead to failure. This is a useful method for understanding the damage development which can be used to model the deformation and fracture behavior. Once a material has completely failed, it is generally difficult to identify the initial or dominant damage mechanisms and the failure evolution. However, a strain controlled interrupted test can be used to explore the influence of loading and morphological parameters on damage evolution. The main reason that this test is suitable for MEA failure evolution investigation is that by performing an interrupted test at different strain levels under uniaxial tension, it is possible to characterize different damage levels and to obtain a detailed quantitative microstructural analysis of the damage evolution [16]. These interrupted tests were conducted in collaboration with Dr. Yaliang Tang.

2.2.2 Material Studied and Experimental Set-Up

In this experimental investigation we investigated a membrane electrode assembly produced by W.L. Gore & Associates in sheets of 49-51 μm thickness to evaluate the failure evolution. These are the same type of MEAs discussed in the previous section. The manufacturing process produces sheets which have two distinct in-plane directions: the machine and transverse directions. The interrupted tests reported here, were conducted in the machine direction. The specimens were cut into rectangular pieces 110 mm in length and 10 mm in width (Fig. 2.3). Each specimen was carefully measured using a caliper to obtain the length and the width, and using a micrometer to measure the thickness.

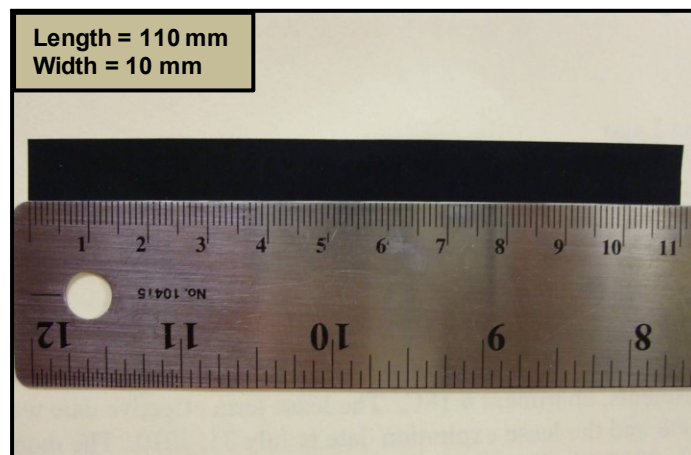


Figure 2.3 Sample of MEA (black) used to conduct an interrupted test. Rectangular piece of dimensions: 110 mm in length and 10 mm in width.

The interrupted tests were conducted at room conditions ($T=25^{\circ}\text{C}$, $\text{RH}=30\%$) using an MTS Alliance TM RT/5 tensile tester (Fig. 1.2). The MTS Alliance TM RT/5 tensile tester is connected to a computer where all the data from the

test is automatically saved. It is possible to start and control the test either by using the computer or by manually controlling the tensile tester. Plots of for example force-displacement and stress-strain curves, can automatically be generated from the recorded data.

The procedure used to mount the specimens in the tensile tester follows that explained in chapter 1 for the tensile test experiments of Membrane A. Since the objective is to investigate the damage evolution and to obtain a detailed microstructural analysis of the failure evolution, the interrupted tests were performed at selected strain levels. Four cases were considered: strain $\Delta L/L = 0.1, 0.2, 0.3,$ and 0.4 . After the specimen was properly mounted in the chamber, displacement-controlled tension was applied on the specimens and the stress-strain relationship was recorded. These results were used as a reference to stop the experiment when the stress-strain curves reached the desired strain value ($0.1, 0.2, 0.3, 0.4$ strain).

2.2.3 Scanning Electron Microscope (SEM)

After the samples were subjected to the interrupted tests up to selected strain levels, a rectangular piece of approximately 6 mm in length and 5 mm in width was cut from each specimen. Each piece of the specimen was evaluated by using a scanning electron microscope. By scanning the specimen surface, this microscope gives information about the sample including external morphology, chemical composition, crystalline structure and orientation of materials making up the sample [17]. A wide range of magnifications is possible, from about 25 x to about 300,000 x [18]. The sample preparation for SEM analysis depends on the nature of the samples and the data required. Specimens must be electrically conductive (at least on the surface). If the sample is electrically insulated, it is usually coated with a thin layer of

conducting material, commonly carbon, gold, or some other metal or alloy [17]. Since the MEA is a layered composite structure, where the upper and lower faces are porous carbon electrodes, there was no need to coat the sample with a conducting material. The samples must fit in the specimen chamber and are generally mounted rigidly on a specimen holder called a specimen stub, which is generally made of aluminum (Fig. 2.4).



Figure 2.4 Aluminum stubs used for taking SEM images.

2.2.4 Results and Discussion

SEM images showing the presence of microstructural deformation, surface damage as well as any potential crack locations were collected. The SEM images were taken from the specimens tested at different strain levels and also from the as-received samples (untested samples) (Fig. 2.5).

Distinct defects can be seen in these images. The observed defects appear as cracks perpendicular to the loading direction (Fig. 2.6). Furthermore, by comparing the different SEM images, it is possible to observe that the number of cracks increases,

and ranges from 20 to 130 cracks per mm along a line parallel to the loading direction as the specimen is pulled (Fig. 2.7).

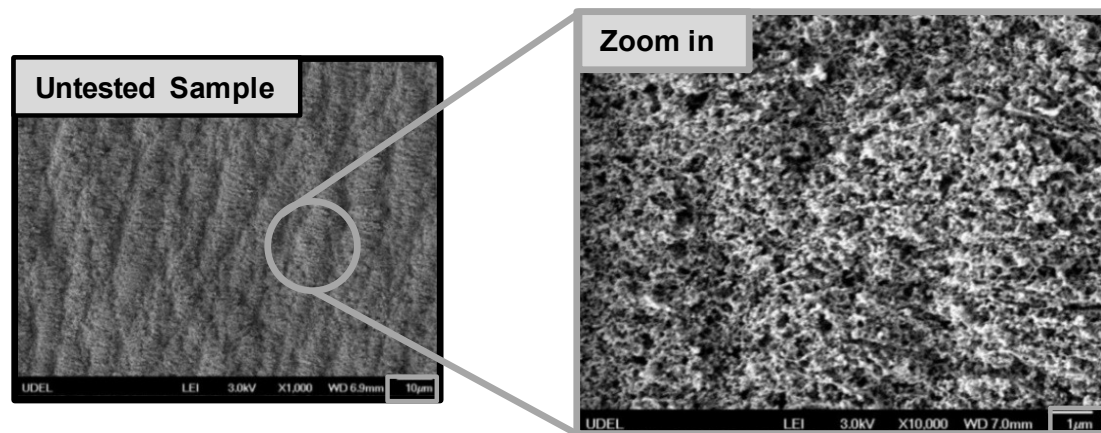


Figure 2.5 SEM image of an untested (as received) MEA sample.

From the images, it is also possible to measure the width of the cracks and the separation between cracks (Fig. 2.8). The width of the cracks increases, ranging from approximately 18 to 200 μm and the separation between cracks decreases from about 10 to 75 μm as the strain is increased. These observations from SEM images at selected strain levels are summarized in table 2.1.

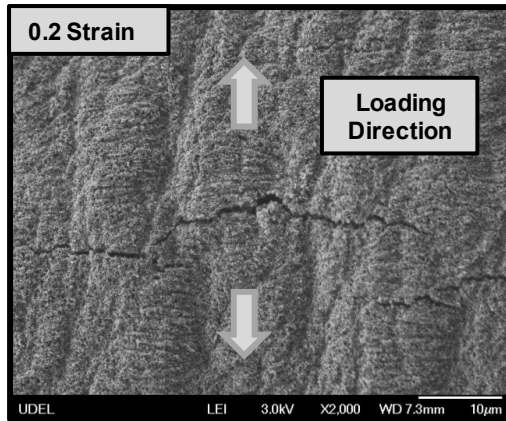


Figure 2.6 SEM image of an MEA sample pulled until 0.2 strain. The cracks are perpendicular to loading direction

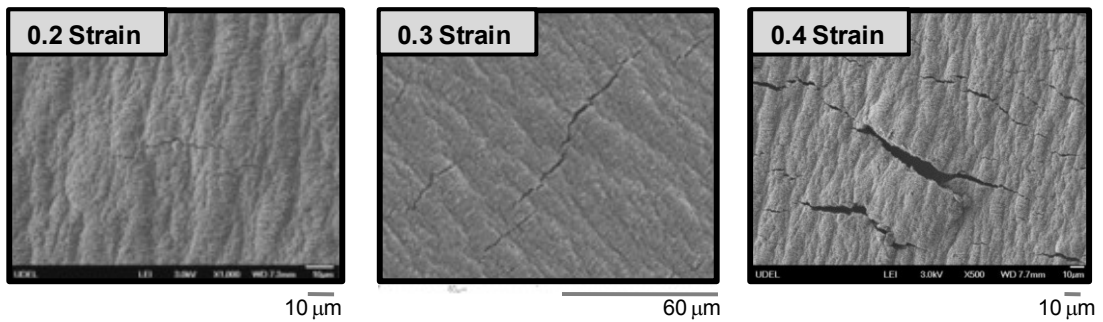


Figure 2.7 SEM images of MEA samples pulled until different strain levels: a) 0.2 strain, b) 0.3 strain, and c) 0.4 strain. Crack density increases as the tension load is applied.

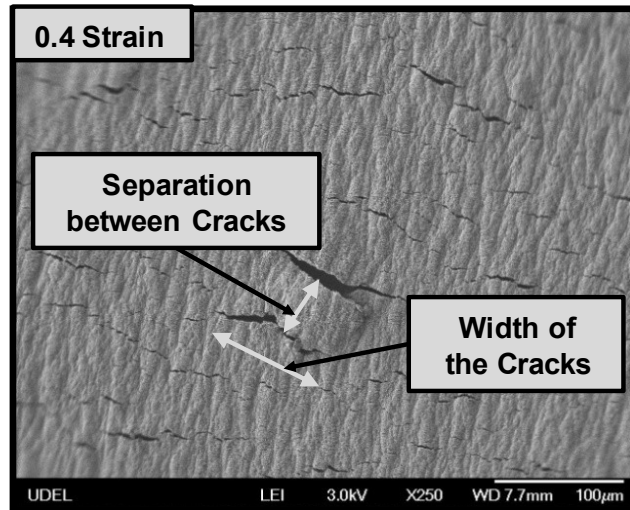


Figure 2.8 SEM image of an MEA sample pulled until 0.4 strain. Separation between cracks and width of the cracks are illustrated.

Table 2.1 Observations from SEM images at selected strain levels.

| | Strain 0.2 | Strain 0.3 | Strain 0.4 |
|-------------------------|---------------------|---------------------|----------------------|
| # of Cracks per mm | 20 | 50 | 130 |
| Width of the Cracks | 18-50 μm | 18-78 μm | 25-200 μm |
| Distance between Cracks | 10 μm | 33-75 μm | 10-60 μm |

The SEM images are taken of the surface of the electrodes with the cracks going perpendicular to the surface, through the electrode and possibly through the membrane. However, from the SEM images it is not possible to determine the length (depth normal to the surface) of the cracks. Cross section images of MEA samples are needed in order to determine the length of the cracks.

2.3 Synopsis

The presence of cracks in MEA, and their increase in quantity and width as the strain is applied, suggests a continuous degradation process on the MEA and their constituents. Possibly, interfacial delamination between membrane and electrode is also present, arising different interfacial stresses between the membrane and electrode in the MEA. Damage, in the form of cracks and delaminations, causes reduction in stiffness and strength, which can lead to failure in the overall structure. This strain controlled interrupted testing technique was used to obtain a quantitative measure of the evolution of the microscopic damage that can cause failure in MEA and eventual failure in the fuel cell as a whole. Based on these results, and in conjunction with tensile test results, the aim in the next chapter is to investigate, by using finite element simulations, how crack density, crack length, and interfacial delamination influence the mechanical behavior of MEA. In addition, the mechanical properties of the electrodes and their influence on the mechanical response of the MEA are also investigated in order to consider a wide spectrum of possibilities that can lead to failure in the MEA.

Chapter 3

NUMERICAL WORK

3.1 Model Description

3.1.1 Introduction

Increasing PEMFC durability and competitiveness requires better understanding of the damage development process and determining of the mechanical behavior of the MEA and its components. Previous tensile tests, discussed in Chapter 1 and 2, were useful in determining the mechanical behaviors of the MEA and membrane A under different operating conditions. Results from these experiments show that many parameters, including fuel cell operation temperature and relative humidity, have a significant effect on the mechanical response of the MEA. Moreover, by performing a strain controlled interrupted test, explained in Chapter 2, the evolution of microstructural damage in the MEA was investigated. Many premature failures in PEM fuel cells are attributed to the formation of cracks due to mechanical stresses [19]. Also, the nonuniform distribution of stresses can contribute to the formation of cracks and/or delamination [10]. By conducting interrupted tests at selected strain levels, a common feature among all the analyzed samples was observed. The development of cracking on the surface of the electrodes was a distinct defect observed among all the samples. Although a fuel cell can still operate in the presence of cracking in the electrodes, the performance and durability can be negatively affected

by this degradation. These electrode cracks can lead to cracks in the membrane and delaminations, which can cause overall failure of the fuel cell. The results from these interrupted tests were used to understand and model the deformation and fracture behavior.

The material properties and mechanical response of Membrane A was investigated in ref. [9] and summarized in Chapter 1. Moreover, the mechanical response of the MEA based on Membrane A was discussed in Chapter 2. In this chapter, the mechanical response of the MEA will now be investigated through simulations. Since the MEA exhibits a highly non-linear response (Fig. 1.5), including plasticity and cracking, the study can not be conducted by using analytical methods. Thus, based on the data and observations from tensile and interrupted tests, we create a finite element model simulating the test conditions in order to investigate the mechanical response and damage evolution of PEM electrodes. Reverse finite element analysis is used in order to determine the mechanical properties of PEM electrodes. Several phenomena are investigated numerically: influence of crack density, influence of crack length, influence of interfacial delamination, and influence of plasticity in the electrodes. Using this methodology, the constitutive behavior of the MEA with damage can be described by matching the experimental and numerical results.

3.1.2 Geometry

A two-dimensional finite element model was developed using the commercial software ABAQUS 6.7 [20]. The model corresponds to a typical segment of the Membrane Electrode Assembly (MEA) (Fig. 3.1). Using symmetry, only a quarter of the structure is modeled, reducing the model size and consequently computational time. Symmetric boundary conditions, $u_y=0$ at the bottom edge and

$u_x=0$ on the left edge are applied. The boundary conditions along the right edge are prescribed so that all the coordinates move uniformly in the x-direction. The loading is applied as a constant horizontal displacement on this edge.

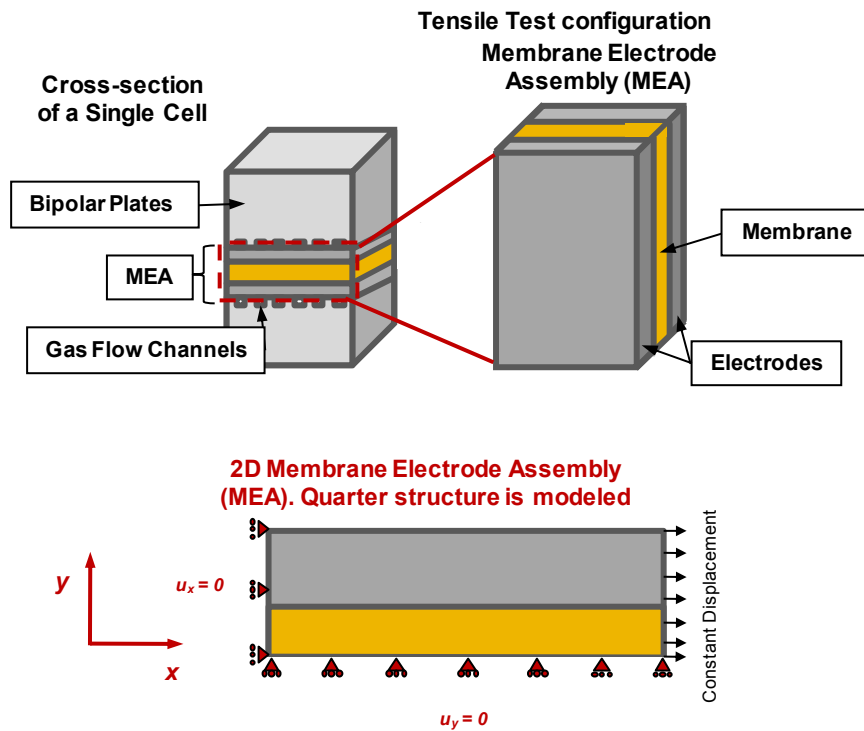


Figure 3.1 Schematic representation of a single fuel cell and the model investigated. A quarter of the geometry of the MEA is used in the numerical analysis. Mechanical boundary conditions are shown. A constant displacement is applied on the right edge of the cell.

The membrane and electrode are each modeled as isotropic and homogeneous materials. Where there is no delamination, the two layers are assumed

perfectly bonded along the uncracked interface. The length of the reference MEA model is 1 mm. The thickness of the MEA is 0.0245 mm, where 0.011 mm corresponds to the thickness of the membrane and 0.0135 mm corresponds to the thickness of the electrode. Eight-node generalized plane strain biquadratic quadrilateral reduced integration elements, CPEG8R, are used. A schematic figure of the model with its corresponding dimensions is shown in Fig. 3.2.

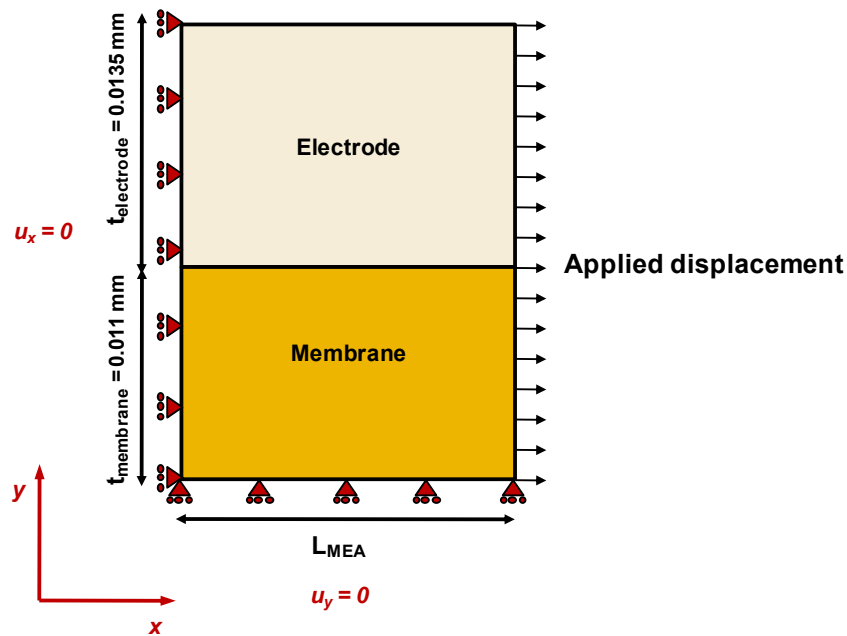


Figure 3.2 Schematic representation of the finite element model and its corresponding dimensions.

As previously mentioned, the mechanical response of Membrane A was investigated in ref. [9] (summarized in Chapter 1) and the mechanical response of a

MEA based on Membrane A was discussed in Chapter 2. The properties of the membrane alone, taken from tensile test results, are assumed unchanged by the addition of the electrodes and are used as input in the finite element model. As mentioned previously, the purpose of this work is to determine the mechanical properties of the electrodes. The question is: If the membrane properties are known, what are the properties of the electrode that would result in the measured response of the MEA?. We will use a reverse analysis to estimate these properties. To this end, the properties of the electrodes are varied in the numerical model until the MEA's numerical curve matches the MEA's experimental curve.

Within the linear-elastic range, the mechanical properties are given by Young's modulus and Poisson's ratio. The rule of mixture for iso-strain condition can be used to determine the elastic properties of the electrodes. This rule is based on the assumption that when a tensile load is applied parallel to the constituents of a sandwich composite, it can be assumed that the strains of the constituents and the composite in the loading direction are the same

$$\varepsilon_{\text{MEA}} = \varepsilon_{\text{m}} = \varepsilon_{\text{e}} \quad (3.1)$$

A simple free body diagram of the MEA easily reveal that the resultant force of the composite F_{MEA} is

$$F_{\text{MEA}} = F_{\text{m}} + F_{\text{e}} \quad (3.2)$$

where F_{m} and F_{e} indicate the force in the membrane and the electrode, respectively.

Furthermore, assuming uniform uniaxial (1-D) stress distribution and considering Hooke's Law,

$$\sigma_{\text{MEA}} A_{\text{MEA}} = \sigma_m A_m + \sigma_e A_e \quad (3.3)$$

$$\sigma = E\varepsilon \quad (3.4)$$

We get,

$$(E\varepsilon A)_{\text{MEA}} = (E\varepsilon A)_m + (E\varepsilon A)_e \quad (3.5)$$

where σ , E , ε , and A indicate the stress, Young's modulus, strain and area, respectively. The subscript m and e indicate membrane and electrode, respectively.

Since the strain of all the constituents is assumed to be identical (a continuity condition), the following simple linear relationship is obtained

$$(EA)_{\text{MEA}} = (EA)_m + (EA)_e \quad (3.6)$$

Equation (3.6) is known as the rule of mixture for iso-strain condition and only applies for linear-elastic response [21]. This equation was used to estimate Young's Modulus of the electrodes based on the experimental known values of Young's Modulus for MEA and membrane. For the two materials (membrane and electrode), Poisson's ratio is assumed 0.4. For the membrane, this value was chosen based on experimental results [22] obtained by conducting tests on perfluorosulfonic acid (PFSA) membranes, which is the most commonly used membrane in PEM fuel cells. From these experiments, Poisson's ratio was set to 0.4. This value was assumed the same for the electrode (porous carbon electrode). A sensitivity analysis was conducted, which showed that differences in the Poisson's ratio have only a small effect on the numerical results.

3.1.3 Constitutive Equations

For the constitutive response beyond the elastic region, the experimental values are matched via FEA. True stress and true strain relationships must be used, since large deformations are considered. True stress σ_{true} and true strain ϵ_{true} , can be related to engineering stress σ_e and engineering strain ϵ_e according to

$$\sigma_{\text{true}} = (1 + \epsilon_e) \sigma_e \quad (3.7)$$

$$\epsilon_{\text{true}} = \ln(1 + \epsilon_e) \quad (3.8)$$

From the experimental results, it can be seen that both the MEA and the membrane have a highly non-linear response after the initial linear region (Fig. 1.5). Based on the membrane results [9], linear-elastic, followed by plastic response with isotropic hardening material properties are used to simulate the membrane response. The isotropic hardening used in ABAQUS is defined by the initial yield stress, where the plastic strain is assumed to be zero and several additional stress points input by the user. The corresponding values are shown in table 3.1.

To determine the mechanical properties of PEM electrodes, the properties of the electrodes are varied in the FEA. When the numerical results of the MEA agree with the experimentally obtained constitutive response, we can assume that the properties used numerically correspond to the properties of the electrodes. Initially, linear-elastic electrodes are assumed by using, as mentioned before, the rule of mixture for iso-strain condition to obtain Young's modulus. Furthermore, both perfect plasticity and plasticity with isotropic hardening behavior are also considered.

Table 3.1 Isotropic hardening values for membrane A based on tensile test results.

| σ_y (MPa) | ϵ_p |
|------------------|--------------|
| 18.4601 | 0 |
| 27.9205 | 0.0858 |
| 36.1536 | 0.1646 |
| 44.9960 | 0.2375 |
| 53.9596 | 0.3060 |
| 62.1471 | 0.3699 |
| 69.2221 | 0.4297 |
| 75.5110 | 0.4862 |
| 80.7199 | 0.5400 |

3.1.4 Cases Studied

Based on the experimental results from the interrupted tests, where cracks were observed among all the analyzed samples (Fig. 2.5), the presence of cracks is studied using finite element simulations. Influence of crack density, crack length, and interfacial delamination are all investigated. The effect of these failure modes on the mechanical response of the MEA is analyzed through numerical simulations and compared with the experimental results.

The geometry of the model varies depending on the case studied. Four cases are modeled: selected crack densities, selected crack lengths, selected delamination lengths, and selected mechanical properties for the electrodes. For each case, the necessary mesh density was determined by repeated mesh refinement until

the results converged. A very fine mesh was used in the zone near to the crack and/or delamination with a coarser mesh used in the undamaged regions.

3.1.4.1 Influence of Plasticity

For the finite element model, mechanical properties from membrane and electrodes are used as input. Elasto-plastic behavior with isotropic hardening properties are used for the membrane, based on tensile test results [9]. The purpose of this study is to determine the properties of the electrodes by varying the electrode properties in the finite element analysis. When the numerically obtained constitutive behavior matches the one captured experimentally, the properties used in the numerical code are assumed to be the actual properties of the electrode. Initially, linear-elastic electrodes are assumed, where Young's modulus is obtained by using the rule of mixture for iso-strain condition. Then, linear-elastic perfectly-plastic electrodes are assumed. The yield stress for the electrodes σ_y^e is chosen based on MEA and membrane experimental data. A range of σ_y^e was investigated, which resulted in similar results. Table 3.2 shows Young's modulus and the selected yield stress σ_y^e . This table also shows the values for MEA and membrane. Both the membrane and MEA values were obtained from experimental tests (Fig. 3.5).

Table 3.2 Values for Young's Modulus and Yield Stress.

| | T=25°C RH=30% | |
|-------------------|----------------------|------------------------------------|
| | E (MPa) | σ_y (MPa) |
| MEA | 322.37 | 11.11 |
| Membrane | 584.84 | 18.57 |
| Electrodes | 108.51 | 3.65 |

Table 3.3 Plasticity with strain hardening properties for the membrane and the electrode, where σ_y and ϵ_p indicate the yield strength and plastic strain respectively. These values are used as input in the finite element code.

| Plasticity with Strain Hardening Properties | | | | | |
|--|--------------|--|--------------|---|--------------|
| Membrane | | Electrode | | | |
| From Tensile Tests | | Following the response of the MEA | | Following the response of the membrane | |
| σ_y | ϵ_p | σ_y | ϵ_p | σ_y | ϵ_p |
| 18.4601 | 0 | 3.65 | 0 | 3.65 | 0 |
| 27.9205 | 0.0858 | 9.60 | 0.01969 | 5.52 | 0.0858 |
| 36.1536 | 0.1646 | 10.65 | 0.05518 | 7.15 | 0.1646 |
| 44.9960 | 0.2375 | 11.46 | 0.08708 | 8.90 | 0.2375 |
| 53.9596 | 0.3060 | 12.44 | 0.11850 | 10.67 | 0.3060 |
| 62.1471 | 0.3699 | 13.05 | 0.14620 | 12.29 | 0.3699 |
| 69.2221 | 0.4297 | 13.29 | 0.17260 | 13.69 | 0.4297 |
| 75.5110 | 0.4862 | | | 14.93 | 0.4862 |
| 80.7199 | 0.5400 | | | 15.96 | 0.5400 |

Finally, plasticity with isotropic hardening behavior is assumed for the electrodes in order to have a complete spectrum of the effect of plasticity on the mechanical response of MEA. Two distinct strain hardening responses are assumed for the electrodes. The curves are assumed to follow the shape of the stress-strain response of the MEA and the membrane respectively only lower than the MEA curves (Fig. 3.5). The hardening values corresponding to these two curves (Fig. 3.6) are used as input in the finite element model. The properties used for the membrane and the electrode are summarized in table 3.3, where σ_y and ϵ_p indicate the yield strength and plastic strain respectively.

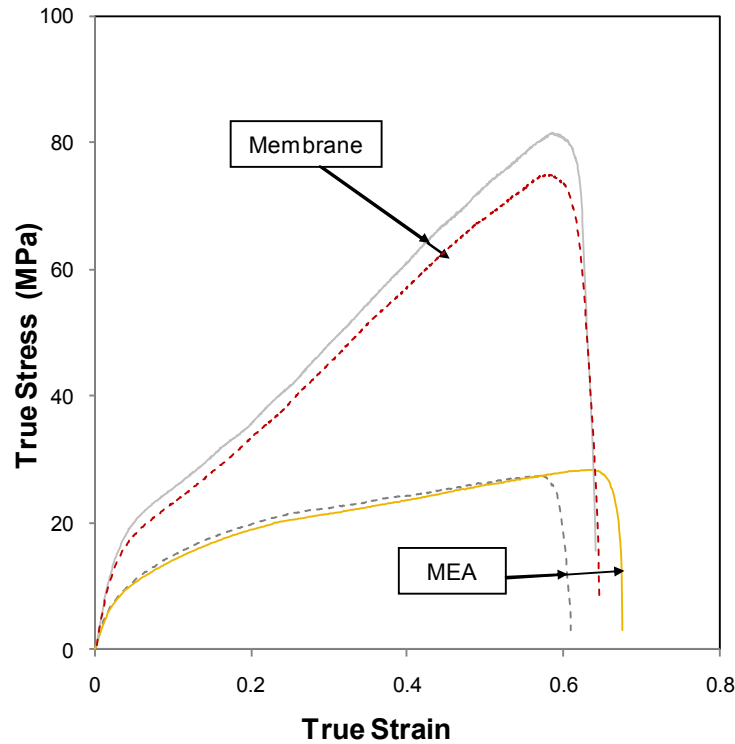


Figure 3.5 Tensile test results for MEA and Membrane at $T=25^{\circ}\text{C}$ and $\text{RH}=30\%$.

3.1.4.2 Influence of Crack Density

In this section, the mechanical behavior of electrodes containing cracks will be investigated. In the MEA, the failure mechanisms appear to be localized and mainly due to mechanical degradation [13]. The most likely sites for crack initiation, are manufacturing flaws which are naturally distributed throughout the MEA. According to experimental tensile test results, the mechanical response of the MEA and the membrane are strongly dependent on operating conditions such as temperature and relative humidity [9]. Furthermore, results from fuel cell experiments indicate that

cracks appear in areas where the MEA is thermally and mechanically overstressed [8]. These cracks, produce areas where there are high local stresses, which have a significant effect on MEA and fuel cell degradation process. Even though fuel cells can still operate in the presence of cracks in the electrodes, the performance and lifetime are affected.

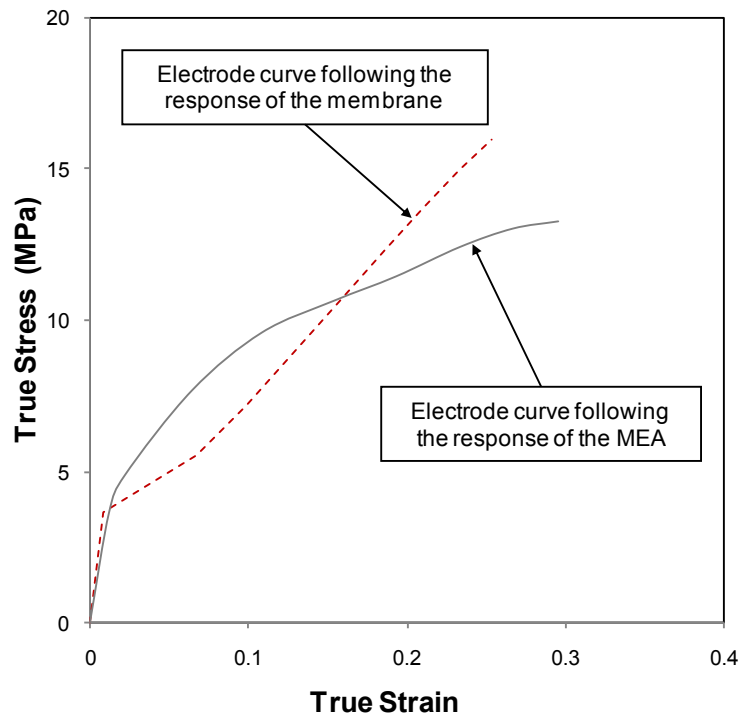


Figure 3.6 Plasticity with strain hardening response assumed for the electrode following the response of the MEA and the membrane respectively.

From the strain controlled interrupted test results (Chapter 2), the damage development process was investigated through SEM images. Distinct defects were seen on the SEM images. The observed defects are cracks perpendicular to the loading direction in the plane (Fig. 2.4). The images also reveal that the number of cracks increases as the extension is increased and ranges from 20 to 130 cracks per mm (table 2.1). Based on these observations, the influence of crack density is studied using finite element simulations.

The effect of crack density on the mechanical response of the MEA is investigated by considering different numbers of cracks in the model. Finite element models are developed corresponding to the different levels of crack density. The length of the MEA model was varied to simulate various crack densities. If a crack density of 1 crack/mm is to be modeled, the length of the MEA model is made to be 0.5 mm since a half model is considered. In a similar manner, 2 cracks/mm requires a 0.25 model length, and so on. In figure 3.7, finite element models corresponding to 4, 32, 64, and 128 cracks per mm are displayed to illustrate the different lengths of the models and their corresponding number of cracks. For all the cases discussed here, the crack length (depth through the plane) is assumed to go all the way through the electrode, e.g., the length of the cracks is assumed to be equal to the thickness of the electrode.

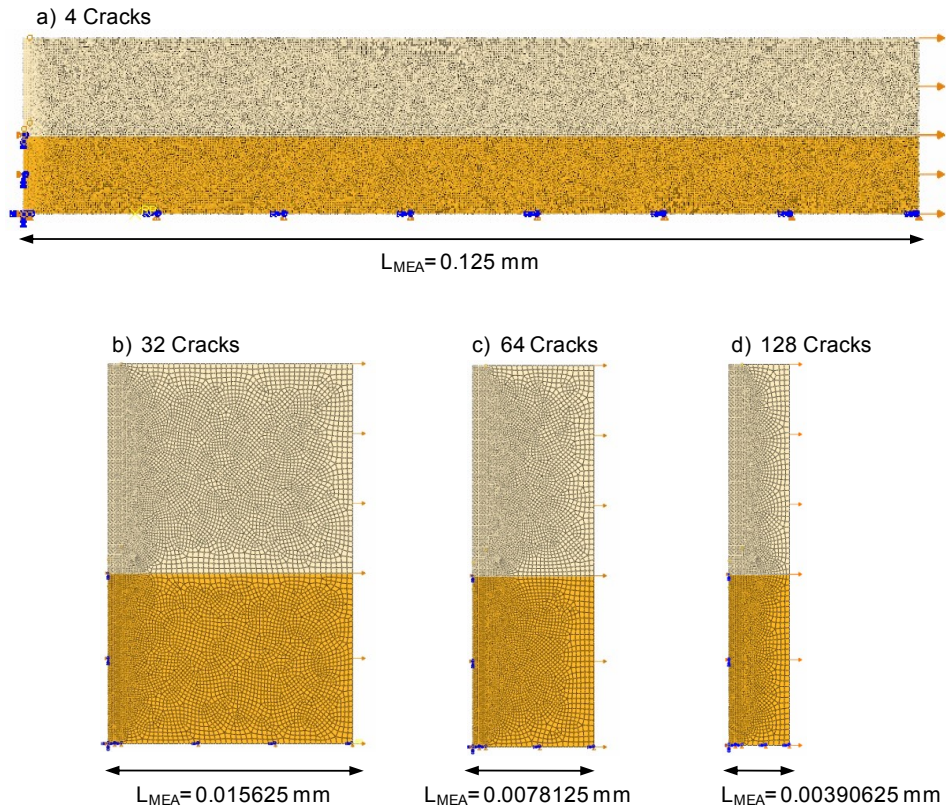


Figure 3.7 Finite element models of MEA generated for studying the influence of crack density on the mechanical response: a) 4 Cracks per mm, b) 32 Cracks per mm, c) 64 Cracks per mm, d) 128 Cracks per mm.

3.1.4.3 Influence of Crack Length

From the SEM images, the crack density, the width of the cracks, and the separation between them could be measured. However, it was not possible to measure the length or depth of the cracks through the electrode from the SEM images. In an attempt to investigate failure evolution, the influence of crack length is of special interest. Eight models are developed, with crack lengths as described in table 3.4.

Furthermore, in figure 3.8, selected finite element models are shown to illustrate the various lengths of crack.

Table 3.4 Different values considered for crack length.

| Length of the Crack (L_{crack}) |
|--|
| 13.75% $W_{\text{MEA}} = 25\% W_{\text{elec.}}$ |
| 27.50% $W_{\text{MEA}} = 50\% W_{\text{elec.}}$ |
| 55.00% $W_{\text{MEA}} = 100\% W_{\text{elec.}}$ |
| 58.00% $W_{\text{MEA}} = 100\% W_{\text{elec.}} + 6.25\% W_{\text{mem.}}$ |
| 61.00% $W_{\text{MEA}} = 100\% W_{\text{elec.}} + 12.5\% W_{\text{mem.}}$ |
| 63.50% $W_{\text{MEA}} = 100\% W_{\text{elec.}} + 18.75\% W_{\text{mem.}}$ |
| 72.00% $W_{\text{MEA}} = 100\% W_{\text{elec.}} + 38.00\% W_{\text{mem.}}$ |
| 80.00% $W_{\text{MEA}} = 100\% W_{\text{elec.}} + 56.00\% W_{\text{mem.}}$ |

3.1.4.4 Influence of Interfacial Delamination.

In addition to cracks through the electrode thickness, delaminations between the electrode and the membrane are possible failure modes. Even small delaminations may affect the integrity and mechanical response of the MEA. Again, the most likely initiation sites for delamination, are manufacturing flaws such as regions of poor adhesion between layers used during manufacturing. The cracks will grow due to stresses caused by the fuel cell operating conditions and severe environmental conditions. Moreover, the differences in properties between the membrane and electrodes can also lead to delamination growth over time [7].

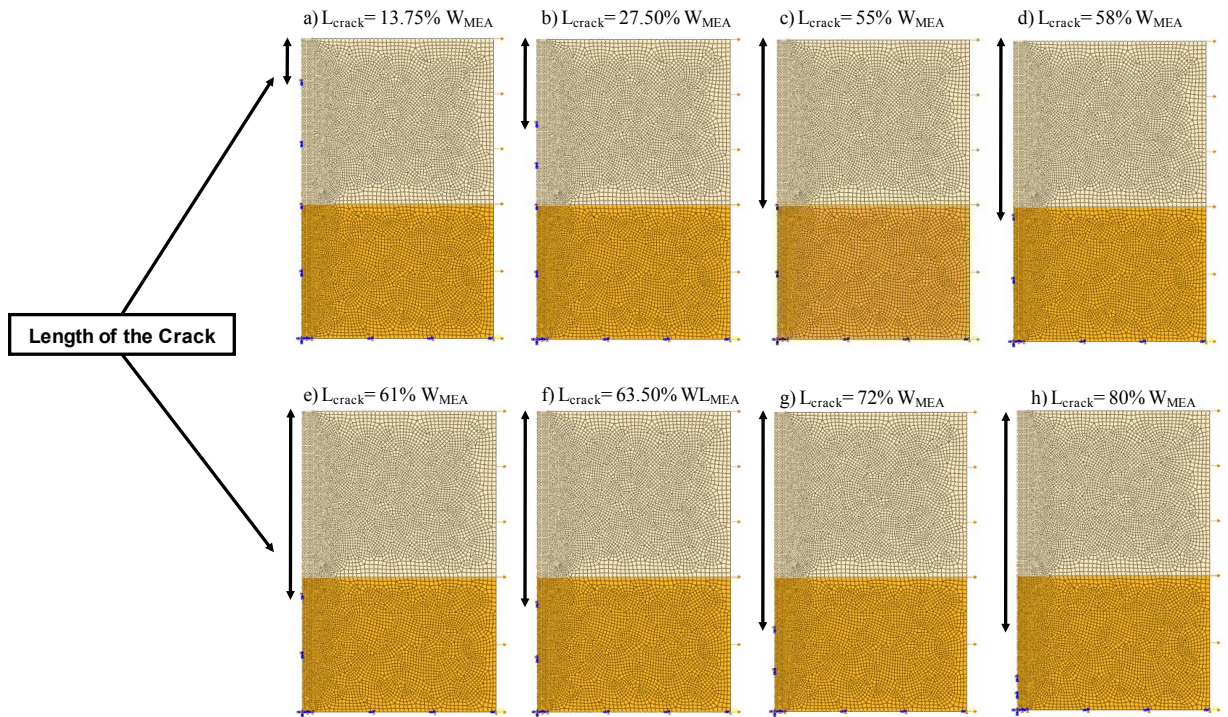


Figure 3.8 Finite element models of MEA generated for studying the influence of crack length on the mechanical response: a) $L_{\text{crack}} = 13.75\% W_{\text{MEA}}$, b) $L_{\text{crack}} = 27.50\% W_{\text{MEA}}$, c) $L_{\text{crack}} = 55\% W_{\text{MEA}}$, d) $L_{\text{crack}} = 58\% W_{\text{MEA}}$, e) $L_{\text{crack}} = 61\% W_{\text{MEA}}$, f) $L_{\text{crack}} = 63.50\% W_{\text{MEA}}$, g) $L_{\text{crack}} = 72\% W_{\text{MEA}}$, h) $L_{\text{crack}} = 80\% W_{\text{MEA}}$. (L_{crack} = Crack Length, W_{MEA} = Width of MEA)

Since our SEM images only reveal information about the surface of the electrodes, there is no information to confirm the presence or absence of delaminations between the membrane and electrodes. It is necessary to get a cross sectional image of the sample in order to see delaminations. However, according to previous studies [23], some defects such as delaminations between the membrane and electrodes, arise in MEAs. In order to fully study the effects of damage, it is necessary to investigate and understand the influence of interfacial delamination on the mechanical response of

MEA. Thus, several different FE models are developed, with varying the interfacial delamination length as a parametric way to study such defects. Table 3.5 shows the delamination lengths selected for the parametric study. Furthermore, in figure 3.9, the finite element models are shown to illustrate the different lengths of delamination.

Table 3.5 Different values considered for the interfacial delamination length.

| Length of Delamination (L_{delam}) |
|--|
| 0.0004219 mm = 2.70% L_{MEA} |
| 0.0008438 mm = 5.40% L_{MEA} |
| 0.003125 mm = 20% L_{MEA} |
| 0.00625 mm = 40% L_{MEA} |

3.2 Results and Discussion

In this section, we will present the numerical results from the finite element simulations. The effect of crack density, crack length, interfacial delamination, and plasticity in the electrodes will be discussed. The numerically generated load-displacement curves will be compared with the experimental results (Fig. 2.2). The experimental results (described in chapter 2) that will be shown are for two cases, that span the experimental results (e.g, upper and lower bounds).

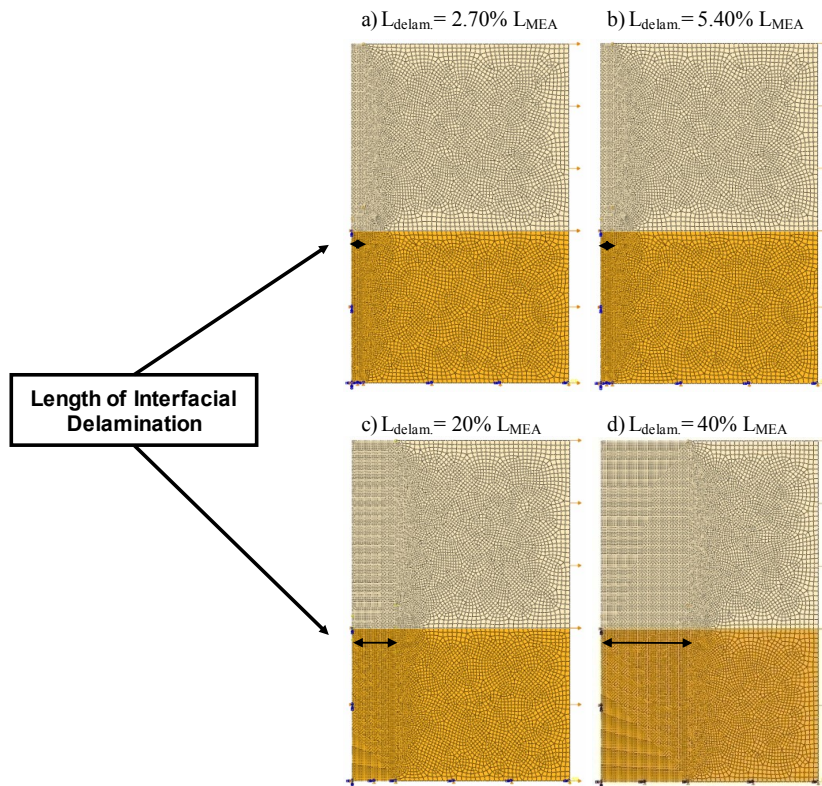


Figure 3.9 Finite element models of MEA generated for studying the influence of interfacial delamination length on the mechanical response: a) $L_{\text{delam.}} = 2.70\% L_{\text{MEA}}$, b) $L_{\text{delam.}} = 5.40\% L_{\text{MEA}}$, c) $L_{\text{delam.}} = 20\% L_{\text{MEA}}$, d) $L_{\text{delam.}} = 40\% L_{\text{MEA}}$

3.2.1 Influence of Plasticity in the Electrode

First, we discuss how the non-linear, plastic response of the electrode influences the mechanical response of the MEA (table 3.3). Figure 3.10 shows the force as a function of displacement, comparing the experimental results with the numerical results when plasticity is assumed for the electrode.

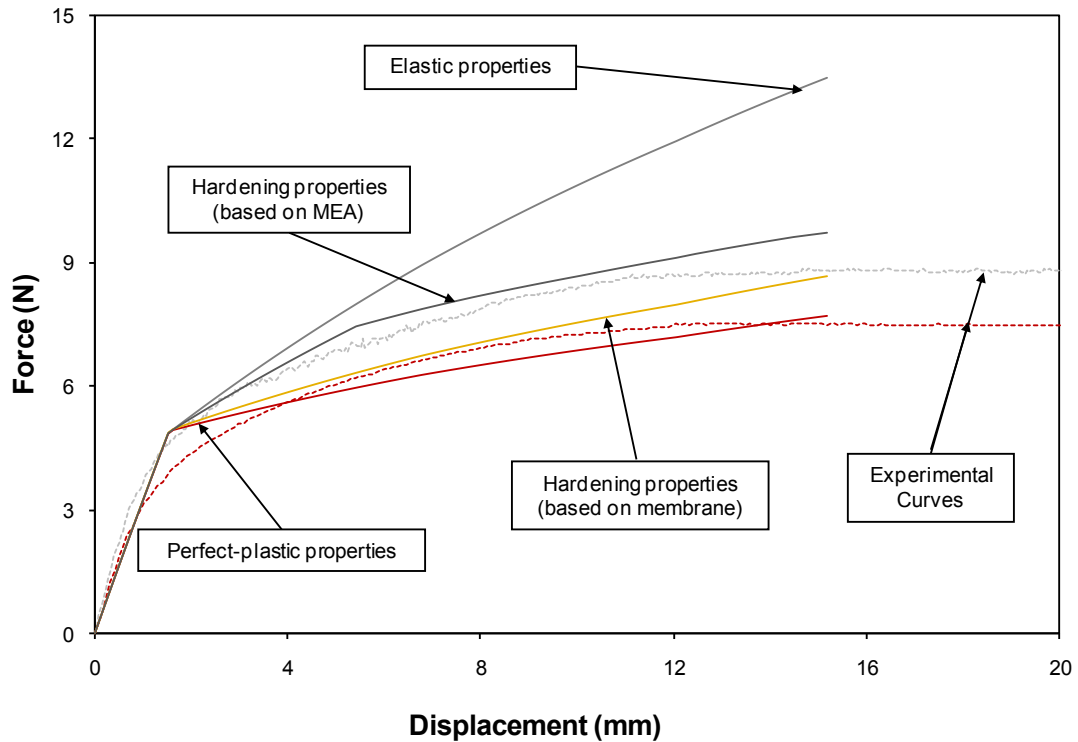


Figure 3.10 Comparison between experimental and numerical results. Numerical curves show the influence of introducing plasticity in the electrodes on the mechanical response of MEA. Numerical model with no cracks.

The numerical results are generated with a finite element model with no cracks. The numerical results suggest that the properties of the electrodes have a strong effect on the mechanical response of MEA. The stiffness of the MEA varies significantly depending on the mechanical properties of the electrodes. We note that using a plastic constitutive law which follows the behavior of the MEA (see section 3.1.4.1) results in the closest fit to the experimental curves.

3.2.2 Influence of Crack Density

In this section, we discuss the influence that the crack density has on the mechanical response of the MEA. For all the cases, the cracks are assumed to go all the way through the electrode, e.g, the crack length is equal to the thickness of the electrode. Figure 3.11 shows the numerically obtained results, displaying force as a function of displacement for selected crack densities: no cracks, 4 cracks, 32 cracks, 64 cracks, and 128 cracks per mm.

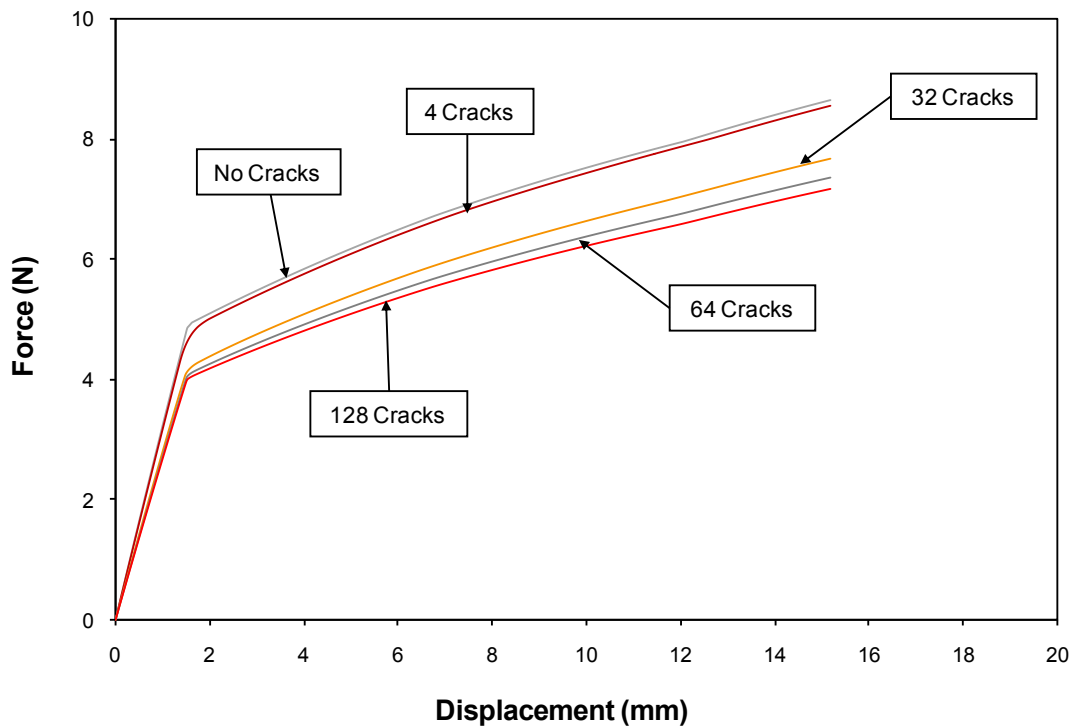


Figure 3.11 Force as a function of displacement from the numerical simulations showing the influence of crack density in the mechanical response of the MEA. Hardening properties for electrodes are assumed based on the constitutive response of the membrane.

Figure 3.12 shows the force as a function of displacement, comparing numerical and experimental results. These simulations were run assuming hardening properties for the electrode, which follow on the constitutive behavior of the membrane (Table 3.3, Fig. 3.6). It can be seen that Young's Modulus decreases as the number of cracks increases.

Numerical simulations are in good agreement with experimental data in the linear elastic region and the beginning of the plastic deformation. However, there is a clear difference between numerical and experimental results in the region of larger deformations.

In the same way, figure 3.13 shows the force as a function of displacement, comparing numerical and experimental results, when perfect plasticity is assumed in the electrodes instead of hardening. In general, the results from both cases indicate that as the number of cracks increases, the stiffness of the MEA decreases.

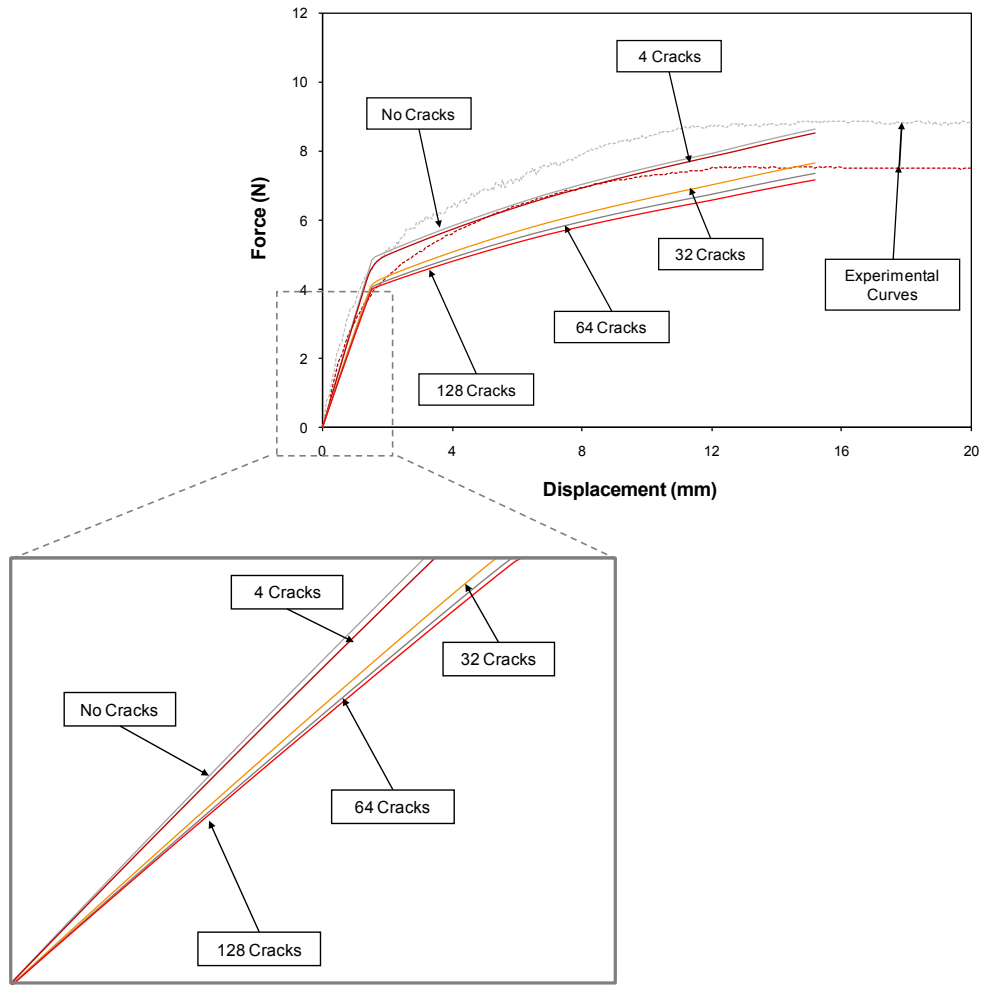


Figure 3.12 Comparison between experimental and numerical results showing force as a function of displacement. Numerical curves show the influence of crack density in the mechanical response of the MEA. Hardening properties for electrodes are assumed to follow the constitutive response of the membrane

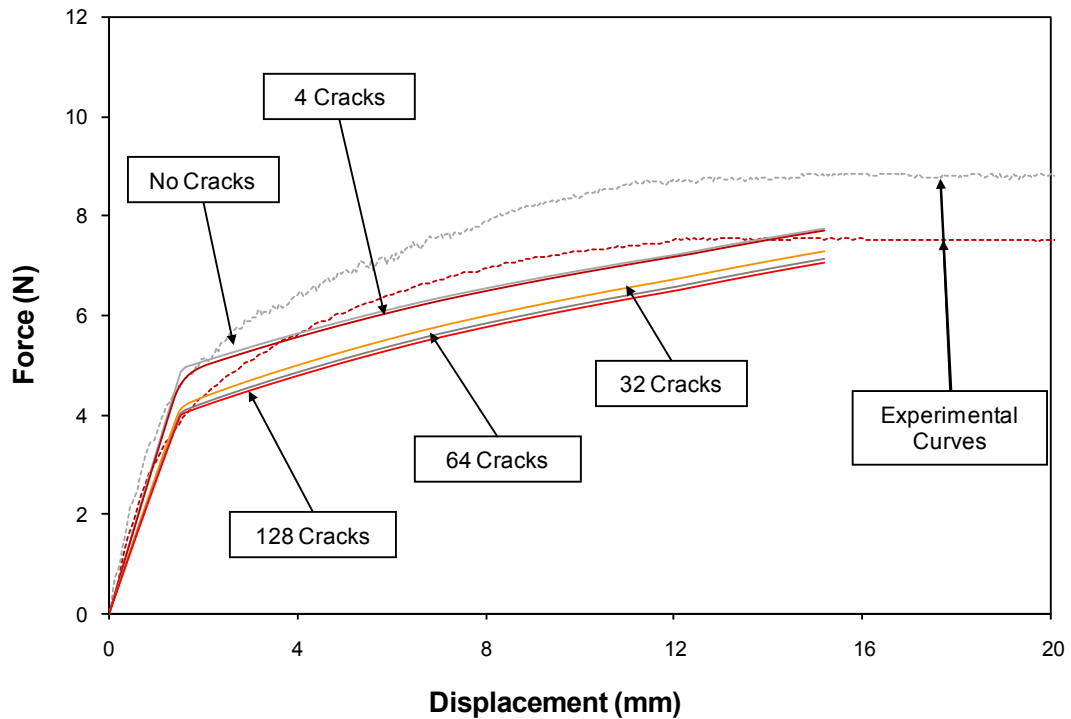


Figure 3.13 Comparison between experimental and numerical results showing force as a function of displacement. Numerical curves show the influence of crack density in the mechanical response of MEA. Electrodes are assumed perfectly plastic.

3.2.3 Influence of Crack Length

In this section, we will investigate the influence that crack length, e.g, the length of the crack through the electrode and possibly through the membrane, has on the mechanical response. For all the cases (table 3.4), thirty two cracks per mm are used and hardening for the electrode is assumed, based on the constitutive response of

the membrane. Figure 3.14 shows the force as a function of displacement for the numerical results compared to the experimental results.

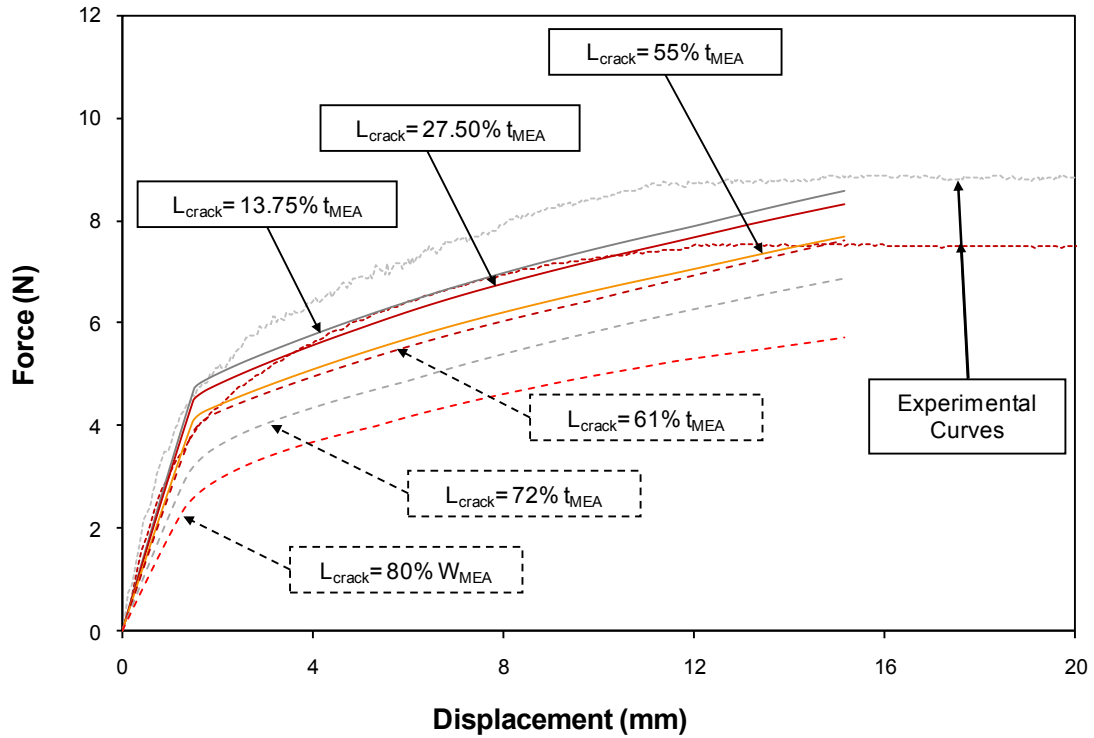


Figure 3.14 Comparison between experimental and numerical results showing force as a function of displacement. Numerical results show the influence of crack length on the mechanical response of the MEA. The numerical curves with solid lines show the influence of cracks through the electrode. The numerical curves with dash lines show the influence of cracks through electrode and membrane. A numerical model with 32 cracks and hardening properties, based on the constitutive behavior of the membrane, for electrodes are assumed.

The numerical results indicate that crack length has a significant effect on the mechanical response of MEA. As the length of the crack increases, the stiffness of the MEA decreases. Moreover, it can be seen that the numerical results with cracks that end at the electrode-membrane interface are in better agreement with the experimental data than the numerical results for cracks going through electrode and partially into the membrane. Thus, we believe that for the experimental cases investigated, the cracks terminate at the electrode-membrane interface and do not propagate into the membrane.

3.2.4 Influence of Interfacial Delamination

Next we investigate the effects of interfacial delamination. Four models are developed, with different interfacial delamination length as summarized in table 3.5. Figure 3.15 shows the force as a function of displacement, where the numerical results are compared to the experimental results.

For all the cases, thirty two cracks and hardening properties, based on the constitutive behavior of the membrane, are assumed for the electrodes. The cracks terminate at the electrode-membrane interface, i.e., crack length equal to electrode thickness. As the length of the interfacial delamination increases, the stiffness of the MEA decreases (Fig. 3.15). The numerical results are in good agreement with experimental data in the linear elastic region. However, the numerical results do not capture the non-linear region of the experimental curves very well. According to the numerical model, increasing delamination length results in decreasing stiffness of the MEA, under-predicting the experimentally measured stiffness of the MEA.

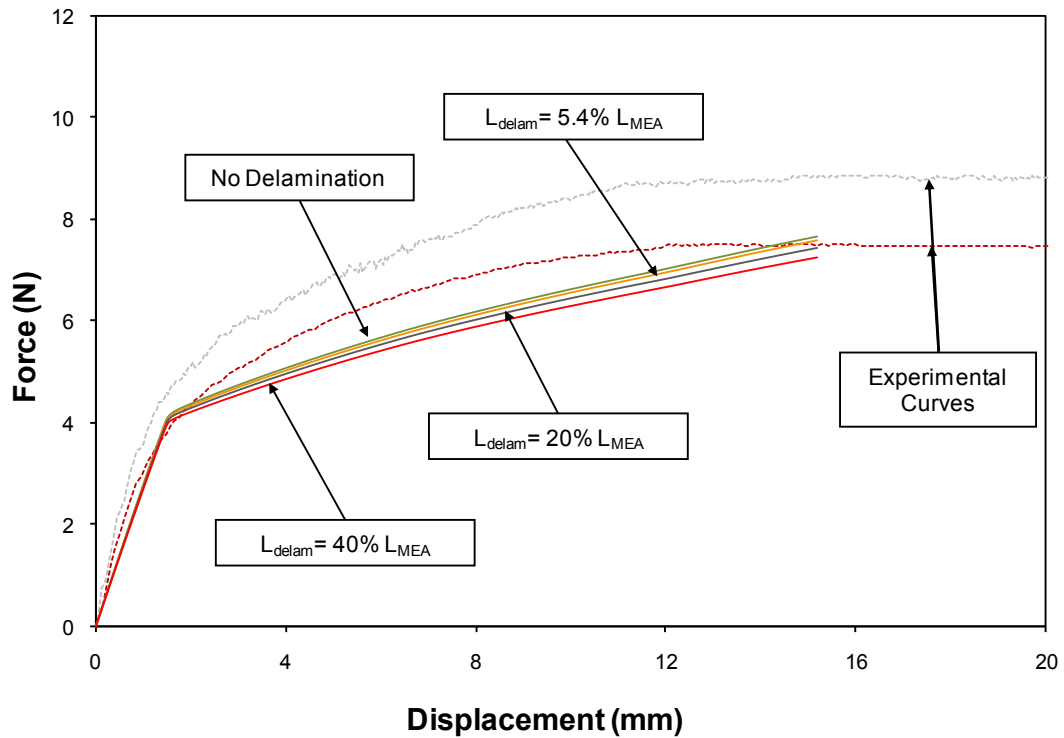


Figure 3.15 Comparison between experimental and numerical results showing force as a function of displacement for various delamination lengths. Numerical model with 32 cracks and hardening properties, based on the constitutive response of the membrane, for electrodes are assumed.

3.2.5 Combined Effects

We will end the discussion by considering numerical simulations where multiple variables are changed. First, we compare the various constitutive responses, investigated in figure 3.16, for the cases of electrodes without cracks and with a crack density of 64 cracks per mm. As previously observed, the mechanical properties of the electrodes have a strong influence on the mechanical behavior of the MEA when there

are no cracks. However, when electrode cracks are present, their influence dominates the overall response (Fig. 3.16). Thus, the mechanical properties of the electrodes seem to have a strong influence on the mechanical response of MEA but the response seems to be dominated by cracks, once they are initiated.

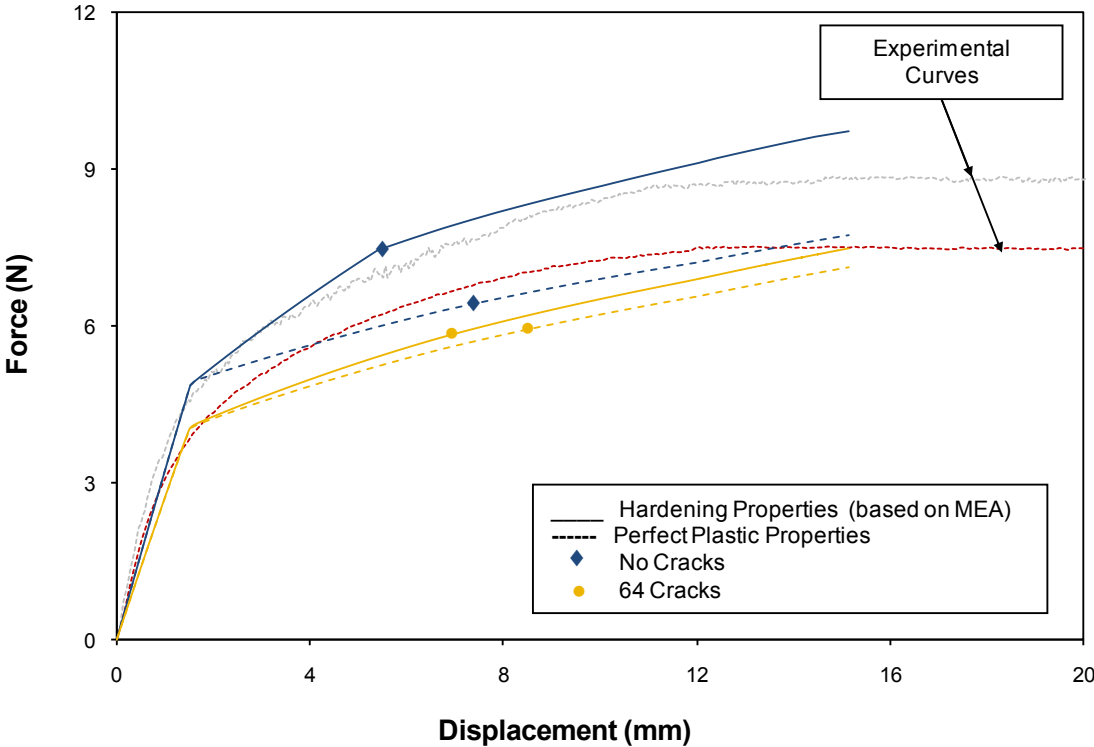


Figure 3.16 Comparison between experimental and numerical results showing force as a function of displacement. Numerical results show the influence of crack density and mechanical properties of the electrodes on the MEA mechanical response.

Lastly, we combine the effects of crack density, delamination, and plasticity on the mechanical response of the MEA. Figure 3.17 compares the numerical results when perfect plasticity and when hardening properties are assumed for the electrode. In addition, crack density and interfacial delamination are also taken into account. Both numerical results, showing force as a function of displacement, are compared with experimental results. From these results, it can be seen that the strongest influence is exerted by the number of cracks contained in the material. Interfacial delamination has a minor effect compared to the effect of crack density. It can be concluded that for the situations considered, crack density has a more dominant effect on the mechanical response of MEA than either the mechanical properties of the electrodes or the length of delamination.

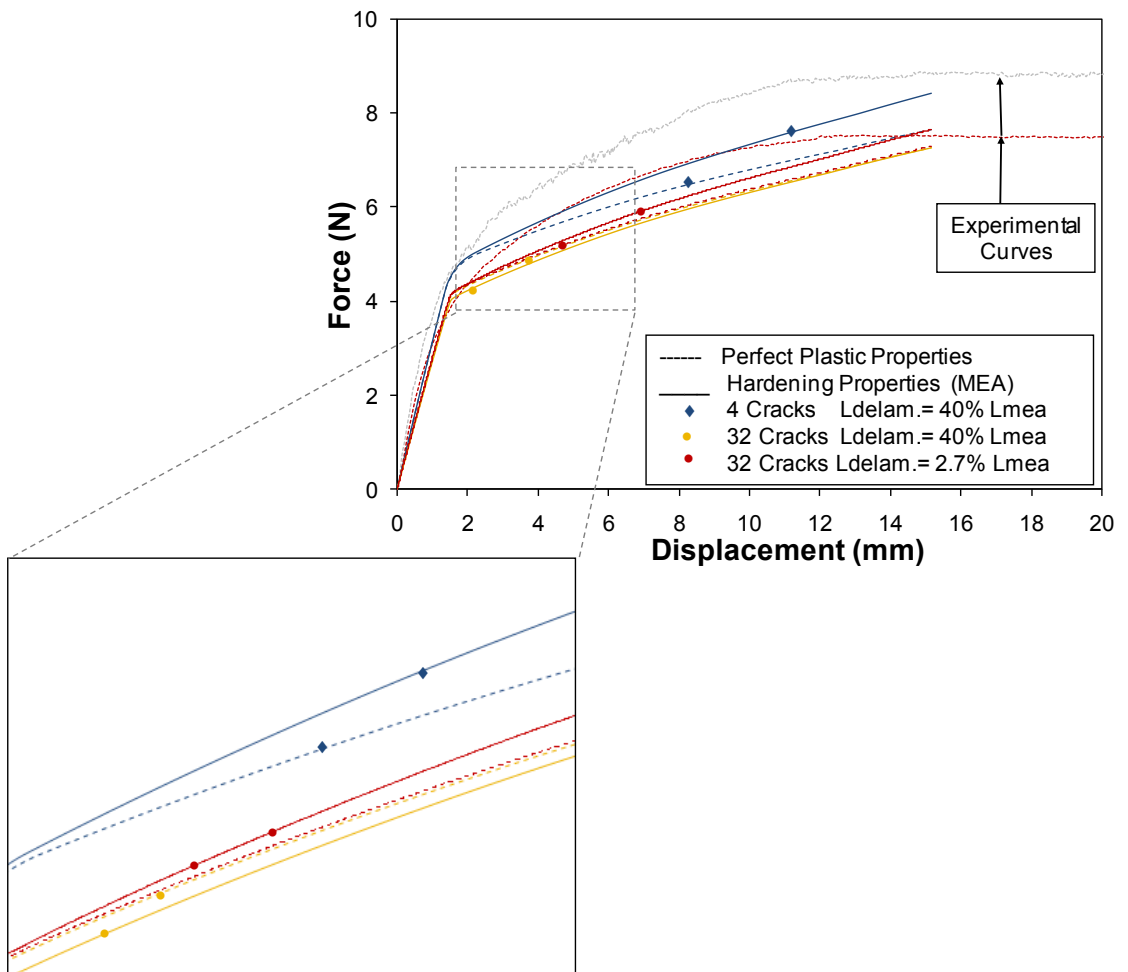


Figure 3.17 Comparison between experimental and numerical results showing force as a function of displacement. Numerical curves show the influence of crack density, interfacial delamination length, and plasticity properties on the mechanical response of MEA, where $L_{del} = 40\% L_{MEA}$.

3.3 Synopsis

Several finite element models have been developed to investigate the damage development process of PEM electrodes and to better understand the MEA mechanical failure evolution. The motivation for this work is to improve the durability in PEM fuel cells. This work has been focused on numerical approximation of experimental results. Comparing numerical simulations with experimental results has been a powerful approach for identifying and understanding the failure evolution.

According to previous work, the nonuniform distribution of stresses can contribute to the formation of cracks and/or delamination [19, 9]. Furthermore, distinct defects such as cracks have been observed experimentally. Previous work, experimental data and observations have been used as the basis for creating the different finite element models in this study.

In general, the finite element simulations are in good agreement with the experimental data in the linear elastic region and the beginning of the plastic deformation. However, numerical and experimental results do not match in the region of larger deformations. However, the developed model, and the cases studied, can capture some of the important features of MEA's mechanical behavior for low to moderate deformation.

The finite element model with cracks terminating at the electrode-membrane interface shows better agreement with experimental data than the model with cracks ending in the membrane. This may suggest that at low to moderate deformation, the cracks in MEAs do not extend into the membrane layer. In addition, the influence of crack density and mechanical properties of the electrodes has been investigated. Perfectly plastic electrodes seem to have the strongest influence on decreasing the stiffness of the MEA. In general, the mechanical properties of the

electrodes seem to have a strong influence on the mechanical response of MEA as long as there are not many cracks, since the effect of cracks dominates. In conclusion, the crack density has a more profound effect on the degradation of mechanical strength of the MEA than either the mechanical properties of the electrodes or the length of delamination.

Chapter 4

CONCLUSIONS

Durability of MEAs has been of great interest in the several past years since it is a major limiting factor in the performance and lifetime of PEMFCs. Different failure modes can arise in the MEA, affecting the durability of the whole fuel cell system. Failure in MEAs can occur in several ways including mechanical damage and chemical degradation. This thesis is focused on some of the mechanical issues linked to the degradation of the MEA, specifically to the degradation of PEM electrodes. We believe that it is important to characterize the mechanical properties and failure evolution of PEM electrodes in order to better understand PEMFC degradation, and consequently develop strategies to increase its durability.

The mechanical behavior of a typical membrane electrode assembly (MEA) has been investigated experimentally. Young's modulus and yield stress have been determined for the MEA by conducting tensile tests. The effects of temperature and humidity on the mechanical properties of the MEA were measured in an environmental control chamber by testing several samples at various temperature and humidity combinations. The results from this work showed that Young's modulus and the proportional limit stress decrease as temperature and relative humidity increase. These results suggest that when the MEA is subjected to a higher temperature and humidity simultaneously, the mechanical behavior is significantly affected.

Since direct testing of the electrodes is not feasible, the failure evolution and the mechanical properties of PEM electrodes have been investigated via a combination of experimental work and numerical simulations. The damage development process in PEM electrodes was investigated by performing strain controlled interrupted tests on MEAs and by observing the resulting damage with a scanning electron microscope. The development of cracks on the surface of the electrodes was a distinct defect observed among all the samples. These cracks appear perpendicular to the loading direction in the plane. The number of the cracks and their width increase as the extension is increased. From the SEM images, it was not possible to determine the length of the cracks (depth through the thickness), since cross section images are needed in order to determine the length. The presence of cracks in MEA, and the increase in quantity and width as the extension is applied, suggests that continuous degradation occurs on the MEA and its constituents.

Having measured the mechanical response of the MEA, the mechanical properties of PEM electrodes were investigated numerically by using reverse analysis and by implementing the previously determined mechanical properties of “Membrane A” in a finite element model, simulating the testing conditions. Based on the tensile test results from “Membrane A” and the MEA, and the SEM observations from PEM electrodes, the objective was to investigate, by using finite element simulations, how crack density, different length of cracks, interfacial delamination, and plasticity in the electrodes influence the mechanical behavior of MEA. A wide spectrum of possibilities that can lead to failure in MEA were studied, by comparing the numerical results from finite element simulations with the experimental results from the MEA tests.

The numerical results suggest that, the properties of the electrodes have a strong effect on the mechanical response of the MEA. The stiffness of the MEA varies significantly depending on the mechanical properties of the electrodes. A plastic constitutive response for the electrodes, which follows the plastic behavior of the MEA, results in the closest fit to the experimental curves. In addition, crack density has a profound effect on the mechanical response of the MEA. Young's modulus decreases as the number of cracks increases. Numerical simulations are in good agreement with experimental data in the linear elastic region and the beginning of the plastic deformation region.

Furthermore, the stiffness of the MEA decreases as the length of the cracks increases. Numerical results are in better agreement with the experimental data when the cracks terminate at the electrode-membrane interface. Thus, we believe that for the cases investigated, the cracks do not propagate into the membrane. Moreover, according to the numerical results, increasing delamination length results in decreasing stiffness of the MEA, underestimating the experimentally determined stiffness of the MEA.

In general, finite element simulations reproduce the experimental results in the linear elastic region and the beginning of the plastic deformation. For larger deformations, numerical results do not capture the behavior observed in the experimental results. However, the model developed was able to capture many important features of MEA's mechanical behavior for the different cases under study. The strongest influence on the mechanical behavior of MEA is given by the number of cracks contained in the material. The mechanical properties of the electrodes also seem to have a strong influence on the mechanical response of MEA but the response is

dominated by cracks, once they are initiated. Interfacial delamination has a minor effect compared to the effect of crack density. In conclusion, the crack density has a profound effect on degradation of the MEA and dominates over the effects of mechanical properties of the electrodes or the length of delamination.

This work was based on a combination of experimental and numerical work that has allowed us to obtain a deeper understanding of the interaction of different factors that affect the mechanical degradation of MEAs and PEM electrodes, and consequently the durability of PEM fuel cells.

REFERENCES

- [1] Mench, M.M. *Fuel Cell Engines*. New Jersey: John Wiley & Sons, Inc., 2008.
- [2] Fuel Cell Systems. 2009. Web site:
http://www1.eere.energy.gov/hydrogenandfuelcells/fuelcells/fc_parts.html
- [3] Morita, T.; Kojima K. *Development of Fuel Cell Hybrid Vehicle in Toyota*. ECS Transactions, 2008. Vol. 16, 185-198.
- [4] Appleby, A.J.; Foulkes, F.R. *Fuel Cell Handbook*. New York: Van Nostrand Reinhold, 1989.
- [5] McDonald R.C.; Mittelsteadt C.; Thompson E. *Effects of deep temperature cycling on Nafion® 112 membranes and membrane electrode assemblies*. Fuel Cells. 2004. Vol. 4, 208-213.
- [6] Collier, A.; Wang, H.; Zi Yuan, X.; Zhang, J.; Wilkinson, D.P. *Degradation of polymer electrolyte membranes*. International Journal of Hydrogen Energy. 2006. Vol. 31, 1838-1854.
- [7] Kundu, S.; Fowler, M.W.; Simon, L.C.; Grot, S. *Morphological features (defects) in fuel cell membrane electrode assemblies*. Journal of Power Sources, 2006. Vol. 157, 650-656.

- [8] Stanic, V.; Hoberecht, M. *Mechanism of pinhole formation in membrane electrode assemblies for PEM fuel cells*. Electrochemical Society Inc., 2004.
- [9] Tang, Y.; Kusoglu, A.; Karlsson, A.M.; Santare, M.H.; Cleghorn, S.; Johnson, W.B. *Mechanical properties of a reinforced composite polymer electrolyte membrane and its simulated performance in PEM fuel cells*. Journal of Power Sources. 2008. Vol. 175, 817-825.
- [10] Tang, Y.; Santare, M.H.; Karlsson, A.M.; Cleghorn, S.; Johnson, W.B. *Stresses in proton exchange membranes due to hygro-thermal loading*. Journal of Fuel Cell Science and Technology, 2006. Vol. 3, 119-124.
- [11] Kusoglu, A.; Karlsson, A.M.; Santare, M.H.; Cleghorn, S.; Johnson, W.B. *Mechanical response of fuel cell membranes subjected to a hygro-thermal cycle*. Journal of Power Sources. 2006. Vol. 161, 987-996.
- [12] LaConti, A.B.; Hamdan, M.; McDonald, R.C. *Handbook of fuel cells- fundamentals, technology and applications*. Vol. 3. New York: John Wiley & Sons, Inc. 2003.
- [13] Liu, W.; Ruth, K.; Rusch, G. *Membrane durability in PEM fuel cells*. Journal of New Materials for Materials for Electrochemical Systems, 2001. Vol. 4, 227-231.

- [14] Zhang, S.; Yuan, X.; Wang, H.; Merida, W.; Zhu, H.; Shen, J.; Wu, S.; Zhang, J. *A review of accelerated stress tests of MEA durability in PEM fuel cells*. International Journal of Hydrogen Energy. 2009. Vol. 34, 388-404.
- [15] Kusoglu, A.; Karlsson, A.M.; Santare, M.H.; Cleghorn, S.; Johnson, W.B. *Mechanical behavior of fuel cell membranes under humidity cycles and effect of swelling anisotropy on the fatigue stresses*. Journal of Power Sources. 2007. Vol. 170, 345-358.
- [16] Li, M.; Ghosh, S.; Richmond, O. *An experimental-computational approach to the investigation of damage evolution in discontinuously reinforced aluminum matrix composite*. Acta mater, 1999. Vol. 47, No. 12, pp. 3515-3532.
- [17] Swaab, S. *Scanning electron microcopy (SEM)*. 2009. Web site:
http://serc.carleton.edu/research_education/geochemsheets/techniques/SEM.html.
- [18] *Scanning electron microcopy (SEM)*. 2005. Web site:
<http://www.siliconfareast.com/SEMTEM.htm>
- [19] Hector, L.G.; Lai, Y.; Tong, W.; Lukitsch, M.J. *Strain accumulation in polymer electrolyte membrane and membrane electrode assembly materials during a single hydration/dehydration cycle*. Journal of Fuel Cell Science and Technology, 2007. Vol. 4.

[20] ABAQUS, ABAQUS Analysis User's Manual version 6.7.

[21] Whitney, J.M.; McCullough, R.L. *Micromechanical Materials Modeling*. Lancaster, Pennsylvania: Technomic Publishing Company, Inc., 1990.

[22] Solasi, R.; Zou, Y.; Huang, X.; Reifsnider, K. *A time and hydration dependent viscoplastic model for polyelectrolyte membranes in fuel cells*. *Journal of Mechanics of Time-Dependent Material*, 2008. Vol. 12, 15-30.

[23] Kushch, V.I; Shmegeera, S.V; Sevostianov, I. *SIF statistics in micro cracked solid: Effect of crack desity, orientation and clustering*. *International Journal of Engineering Science*, 2008. Vol. 47, 192-208.